

การสลายตัวด้วยแสงของสารละลาย 2,4-ไดคลอโรฟีนอล ภายใต้สภาวะแสงขาว
โดยใช้ตัวเร่งปฏิกิริยาซิงค์ออกไซด์ที่ถูกกระตุ้นด้วยเหล็กที่เตรียมโดยวิธีเอ็บซุ่ม



นางสาวประดับดวง เกียรติศักดิ์ศิริ

ศูนย์วิทยทรัพยากร

จุฬาลงกรณ์มหาวิทยาลัย

วิทยานิพนธ์นี้เป็นส่วนหนึ่งของการศึกษาตามหลักสูตรปริญญาวิทยาศาสตรมหาบัณฑิต

สาขาวิชาการจัดการสิ่งแวดล้อม (สหสาขาวิชา)


บัณฑิตวิทยาลัย จุฬาลงกรณ์มหาวิทยาลัย

ปีการศึกษา 2552

ลิขสิทธิ์ของจุฬาลงกรณ์มหาวิทยาลัย

521230

PHOTODEGRADATION OF AQUEOUS 2,4-DICHLOROPHENOL UNDER
VISIBLE LIGHT USING Fe-ZnO CATALYSTS PREPARED BY
IMPREGNATION METHOD



Miss Pradabduang Kiattisaksiri

ศูนย์วิทยทรัพยากร

A Thesis Submitted in Partial Fulfillment of the Requirements
for the Degree of Master of Science Program in Environmental Management
(Interdisciplinary Program)

Graduate School

Chulalongkorn University

Academic Year 2009

Copyright of Chulalongkorn University

Thesis Title PHOTODEGRADATION OF AQUEOUS
2,4-DICHLOROPHENOL UNDER VISIBLE LIGHT USING
Fe-ZnO CATALYSTS PREPARED BY IMPREGNATION
METHOD


By Miss Pradabduang Kiattisaksiri

Field of Study Environmental Management

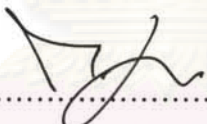
Thesis Advisor Associate Professor Nurak Grisdanurak, Ph.D.

Thesis Co-Advisor Phairat Usubharatana, Ph.D.


Accepted by the Graduate School, Chulalongkorn University in Partial
Fulfillment of the Requirements for the Master's Degree

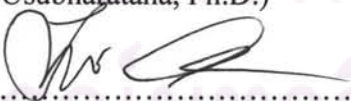

.....Dean of the Graduate School
(Associate Professor Pornpote Piumsomboon, Ph.D.)

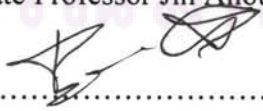
THESIS COMMITTEE


.....Chairman
(Assistant Professor Manaskorn Rachakornkij, Ph.D.)


.....Thesis Advisor
(Associate Professor Nurak Grisdanurak, Ph.D.)


.....Thesis Co-Advisor
(Phairat Usubharatana, Ph.D.)


.....Examiner
(Associate Professor Jin Anotai, Ph.D.)


.....External Examiner
(Panjai Saueprasearsit, Ph.D.)

ระดับดวง เกียรติศักดิ์ศิริ : การสลายตัวด้วยแสงของสารละลาย 2,4-ไดคลอโรฟีนอล ภายใต้สภาวะแสงขาว โดยใช้ตัวเร่งปฏิกิริยาซิงค์ออกไซด์ที่ถูกกระตุ้นด้วยเหล็ก ที่เตรียมโดยวิธีเจือปน. (PHOTODEGRADATION OF AQUEOUS 2,4-DICHLOROPHENOL UNDER VISIBLE LIGHT USING Fe-ZnO CATALYSTS PREPARED BY IMPREGNATION METHOD) อ.ที่ปรึกษาวิทยานิพนธ์หลัก : รศ.ดร.นุรักษ์ กฤษดานุรักษ์, อ.ที่ปรึกษาวิทยานิพนธ์ร่วม : ดร.ไพรัช อู่อภรณ์, 68 หน้า.

ตัวเร่งปฏิกิริยาซิงค์ออกไซด์ที่มีองค์ประกอบของเหล็ก (Fe-ZnO) ถูกเตรียมโดยวิธีเจือปน เพื่อทดสอบการย่อยสลายของสารละลาย 2,4-ไดคลอโรฟีนอลด้วยแสงขาว จากการตรวจสอบคุณลักษณะของตัวเร่งปฏิกิริยาพบว่า เวอร์สไซต์ (wurtzite) เป็นโครงสร้างหลักของ ZnO โดยตัวเร่ง Fe-ZnO มีขนาดผลึกประมาณ 35-40 นาโนเมตร และมีพื้นที่ผิวจำเพาะประมาณ 5-10 ตารางเมตรต่อกรัม คุณสมบัติด้านการดูดกลืนแสงขาวของตัวเร่ง Fe-ZnO มีมากและแปรผันตรงกับปริมาณ Fe สำหรับ Fe ที่เจือลงบน ZnO มีเลขออกซิเดชันเท่ากับ +3 และมีค่าศักย์ซีต้า (zeta potential) บนผิวเป็นศูนย์ที่ pH เท่ากับ 9.5

จากการวิเคราะห์ด้วย Box-Behnken พบว่า สภาวะที่เหมาะสมสำหรับการย่อยสลายสารละลาย 2,4-ไดคลอโรฟีนอลความเข้มข้น 5.0 มิลลิกรัมต่อลิตรภายใต้แสงขาว คือ การใช้ตัวเร่ง Fe-ZnO ที่ความเข้มข้นของ Fe 5.0 โมลเปอร์เซ็นต์ ผ่านการเคลือบที่ 700 องศาเซลเซียส โดยใช้ในปริมาณ 1.5 กรัมต่อลิตรน้ำเสียสังเคราะห์ นอกจากนี้ยังพบว่าการเติมโพแทสเซียมเพอร์ซัลเฟต ($K_2S_2O_8$) สามารถเพิ่มอัตราการย่อยสลาย ภายใต้สภาวะที่เหมาะสมการเติมสารดังกล่าวปริมาณ 2.0 มิลลิโมลาร์ร่วมกับตัวเร่ง Fe-ZnO ทำให้สารละลาย 2,4-ไดคลอโรฟีนอลย่อยสลายได้หมดภายในเวลา 90 นาที ซึ่งมีประสิทธิภาพดีกว่าการใช้ร่วมกับตัวเร่ง ZnO 5 เท่า โดยปฏิกิริยาการย่อยสลายที่เกิดขึ้นสอดคล้องกับทฤษฎีของแลงเมียร์-ฮินเชลวูด

สาขาวิชา การจัดการสิ่งแวดล้อมลายมือชื่อนิสิต ปรัชญว เกียรติศักดิ์ศิริ
 ปีการศึกษา 2552ลายมือชื่อ อ.ที่ปรึกษาวิทยานิพนธ์หลัก
ลายมือชื่อ อ.ที่ปรึกษาวิทยานิพนธ์ร่วม

5187544020 : MAJOR ENVIRONMENTAL MANAGEMENT

KEYWORDS : VISIBLE LIGHT / PHOTOCATALYSIS / Fe-ZnO / 2,4-DCP / BOX-BEHNKEN DESIGN

PRADABDUANG KIATTISAKSIRI : PHOTODEGRADATION OF AQUEOUS 2,4-DICHLOROPHENOL UNDER VISIBLE LIGHT USING Fe-ZnO CATALYSTS PREPARED BY IMPREGNATION METHOD.

THESIS ADVISOR : ASSOC. PROF. NURAK GRISDANURAK, Ph.D.,

THESIS CO-ADVISOR : PHAIRAT USUBHARATANA, Ph.D., 68 pp.

Fe-ZnO catalysts were synthesized by impregnation technique and used to test the photocatalytic degradation of 2,4-DCP under visible light. Catalyst characteristic mainly presented wurtzite structure of ZnO, with crystalline size of 35-40 nm and $5-10 \text{ m}^2 \text{ g}^{-1}$ of specific surface area. Visible absorption of Fe-ZnO catalyst increased proportionally with Fe content. Oxidation state of Fe on ZnO surface was +3 and zero point charge was found at pH 9.5.

Degradation experimental following Box-Behnken analysis provided an optimal condition of 2,4-DCP (initial concentration: 5.0 mg L^{-1}) degradation under visible light at 5.0 mol% Fe-ZnO calcined at 700°C , and catalyst loading of 1.5 g L^{-1} (volume of synthetic waste water). Besides, the addition of 2 mM potassium persulfate ($\text{K}_2\text{S}_2\text{O}_8$) could increase the degradation efficiency and the reaction could be completed within 90 min. The degradation performance on Fe-ZnO combined with $\text{K}_2\text{S}_2\text{O}_8$ was 5 times higher than that using ZnO combined with $\text{K}_2\text{S}_2\text{O}_8$. Reaction kinetics was fitted very well with the Langmuir-Hinshelwood model.

Field of Study : Environmental Management Student's Signature Pradabduang Kiattisaksiri

Academic Year : 2009 Advisor's Signature Nurak Grisdanurak

Co-Advisor's Signature Phairat Usubharatana

ACKNOWLEDGEMENTS

First of all, I would like to express my deepest gratitude to my advisor, Assoc. Prof. Nurak Grisdanurak for his support, guidance and assistance throughout my study. I would also like to thank my co-advisor, Dr. Phairat Usubharatana for his advice regarding my work. Thank all the respective committee members, Assist. Prof. Manaskorn Rachakornkij, Assoc. Prof. Jin Anotai, and Dr. Panjai Saueprasearsit for their stimulating questions and valuable suggestions.

I particularly thank Mr. Kitirote Wantala (Ph.D. student), for his technical assistance in characterization, experimental contributions, and teaching about Minitab software. Thank you for the kind help during my times in the laboratory. I appreciate the support of Dr. Pongtanawat Khemthong (Postdoctoral student), and Mr. Danutawat Tipayarom (Ph.D. student) for suggestions, and valuable advices.

A special thank you goes to Asst. Prof. Laksana Laokiat, and Ms. Pummarin Khamdahsag (Ph.D. student) for many useful tips and great guidance in the experiments. Thank you for the friendship that they always generously offered as well as their encouragement, and beneficial suggestions to support life skills. I also need to thank all staff and my friends in catalyst laboratory, TU and NCE-EHWM, CU for their wonderful assistance.

I am very grateful to NCE-EHWM, Chulalongkorn University, for the financial support. My gratitude is also for Department of Chemical Engineering of Thammasat University for the laboratory usage. Additionally, I am grateful to Synchrotron Light Research Institute for XAS analysis.

Finally and most importantly, I am extremely grateful for the support of my parents and family. Their love and warm encouragement have been my greatest strength and inspiration for my success in the past, now, and in the future.

CONTENTS

	PAGE
ABSTRACT (IN THAI).....	iv
ABSTRACT (IN ENGLISH).....	v
ACKNOWLEDGEMENTS.....	vi
CONTENTS.....	vii
LIST OF TABLES.....	x
LIST OF FIGURES.....	xi
CHAPTER I: INTRODUCTION.....	1
1.1 Motivations.....	1
1.2 Objectives.....	2
1.3 Scopes of the study.....	2
1.4 Expected Outcomes.....	3
CHAPTER II: LITERATURE REVIEW.....	4
2.1 2,4-dichlorophenol (2,4-DCP).....	4
2.1.1 Characteristic of 2,4-DCP.....	4
2.1.2 Human exposure and toxicological effects.....	5
2.1.3 Environmental contamination.....	7
2.1.4 Standards for 2,4-DCP.....	8
2.1.5 Waste treatment technologies.....	9
2.2 Heterogeneous photocatalysis.....	10
2.2.1 Fe-ZnO as photocatalyst.....	10

	PAGE
2.2.2 Photocatalytic reaction.....	14
2.2.3 Photocatalysis of phenolic compounds.....	17
CHAPTER III: MATERIAL AND METHODS.....	20
3.1 Catalyst preparation.....	20
3.1.1 Materials.....	20
3.1.2 Preparation procedures.....	20
3.2 Catalyst characterizations.....	21
3.2.1 X-ray diffraction (XRD)	21
3.2.2 Brunauer-Emmett-Teller (BET) method.....	21
3.2.3 Scanning electron microscopy (SEM)	22
3.2.4 UV-Vis diffuse reflectance spectroscopy (UV-DRS).....	22
3.2.5 X-ray absorption spectroscopy (XAS)	22
3.2.6 Zeta potential analysis.....	23
3.3 Photocatalytic experiment.....	23
3.3.1 Materials.....	23
3.3.2 Photoreactor setup.....	23
3.3.3 Photocatalytic procedures.....	24
3.3.4 Analytical method.....	25
3.3.5 Experimental design and statistical analysis.....	25
CHAPTER IV: RESULTS AND DISSCUSSION.....	27
4.1 Catalyst characterizations.....	27
4.1.1 Structure and crystallite size.....	27

	PAGE
4.1.2 BET surface area.....	29
4.1.3 Surface morphology.....	30
4.1.4 Optical absorption property.....	31
4.1.5 Oxidation state.....	34
4.1.6 Surface charge.....	35
4.2 Photocatalytic testing of 2,4-DCP.....	37
4.2.1 Experimental design analysis.....	37
4.2.2 Kinetic study.....	46
CHAPTER V: CONCLUSIONS AND RECOMMENDATIONS.....	52
5.1 Conclusions.....	52
5.2 Recommendations.....	53
REFERENCES.....	54
APPENDICES.....	62
Appendix A The transmission spectrum of NaNO ₂ solution.....	63
Appendix B Characterization data.....	64
Appendix C Photocatalytic testing data.....	66
BIOGRAPHY.....	68

ศูนย์วิทยทรัพยากร
 จุฬาลงกรณ์มหาวิทยาลัย

LIST OF TABLES

TABLE	PAGE
2.1 Physical and chemical properties of 2,4-DCP.....	5
2.2 International standards for 2,4-DCP.....	8
2.3 Thai's standards for 2,4-DCP.....	9
3.1 The range and level of independent parameters.....	26
4.1 Crystal sizes and surface areas of bare ZnO, and Fe-ZnO samples.....	29
4.2 Box-Behnken design matrix and the response (% degradation).....	38
4.3 Estimated regression coefficients for % 2,4-DCP degradation.....	40
4.4 ANOVA results for % degradation of 2,4-DCP.....	42
B.1 Crystal sizes of the samples.....	64
B.2 The pre-edge energy of the samples and model compounds (FeO, Fe ₂ O ₃). 64	64
B.3 Average zeta potential (mV) of bare ZnO, and Fe-ZnO samples.....	65
C.1 Calibration curve data of 2,4-DCP.....	66
C.2 % degradation of 5.0 mg L ⁻¹ 2,4-DCP at various conditions.....	67
C.3 % degradation of 2,4-DCP at different concentrations.....	67

ศูนย์วิทยทรัพยากร
 จุฬาลงกรณ์มหาวิทยาลัย

LIST OF FIGURES

FIGURE	PAGE
2.1 Chemical structure of 2,4-DCP.....	4
2.2 ZnO crystal structures.....	11
2.3 The e^-h^+ generation in ZnO particle.....	15
2.4 The e^-h^+ recombination process.....	15
2.5 General mechanism of photocatalysis.....	17
3.1 A diagram of Fe-ZnO samples prepared by IW-IMP technique.....	20
3.2 Schematic diagram of the photoreactor.....	24
4.1 XRD patterns of bare ZnO and Fe-ZnO samples at different mol% Fe calcined at 700°C, compared with a standard Fe_2O_3	27
4.2 XRD patterns of bare ZnO and 5.0 mol% Fe-ZnO samples at different calcination temperatures.....	28
4.3 SEM images of the bare ZnO and doped samples (20kX).....	30
4.4 UV-DRS spectra of bare ZnO and Fe-ZnO samples at different Fe contents, calcined at 700°C.....	31
4.5 UV-DRS spectra of bare ZnO and 5.0 mol% Fe-ZnO samples at different calcination temperatures.....	32
4.6 Tauc plots of bare ZnO and Fe-ZnO samples at different Fe contents, calcined at 700°C.....	33
4.7 Tauc plots of bare ZnO and 5.0 mol% Fe-ZnO samples at different calcination temperatures.....	33
4.8 The XANES spectra of doped samples at different Fe contents, calcined at 400°C, and references FeO and Fe_2O_3	34

FIGURE	PAGE
4.9 The XANES spectra of 5.0 mol% Fe-ZnO calcined at various temperatures and references FeO and Fe ₂ O ₃	35
4.10 Plots of the zeta potential as a function of pH for bare ZnO and Fe-ZnO samples at different Fe contents, calcined at 400°C.....	36
4.11 Plots of the zeta potential as a function of pH for bare ZnO and 5.0 mol% Fe-ZnO samples, calcined at 400-700°C.....	36
4.12 Normal probability plots.....	39
4.13 Plot of residual versus fitted value (predicted value).....	40
4.14 A parity plot of % degradation.....	41
4.15 The standardized residual on each run.....	43
4.16 Main effect plots for % 2,4-DCP degradation.....	44
4.17 Contour plots and surface plots on different effects.....	45
4.18 % degradation of 2,4-DCP under various conditions.....	47
4.19 % degradation of 2,4-DCP of 5.0 mol% Fe-ZnO at different initial concentrations.....	49
4.20 Langmuir-Hinshelwood plot depicting linear relationship between 1/r ₀ and 1/C ₀	50
A.1 The transmission spectrum of 1M NaNO ₂ solution.....	63
C.1 Calibration curve of 2,4-DCP.....	66

CHAPTER I

INTRODUCTION

1.1 Motivations

2,4-dichlorophenol (2,4-DCP) is a key intermediate in the synthesis of chloro-pesticides and herbicide. It has been listed among the 120 priority pollutants given by the U.S.EPA in the federal Clean Water Act (United States Environmental Protection Agency [U.S.EPA], 2002 : online). It is a toxic chlorinated compound that is potential carcinogenic, and disturbs human and animal's endocrine system (International Agency for Research on Cancer [IARC], 1999 : online ; Zhang et al., 2005). It is important organic contaminants frequently found in aquatic environment due to its widespread uses in agricultural, petrochemical, dye stuff, and pesticidal chemical industries. 2,4-DCP is quite stable and remains in the environment for long period. Therefore, there is a need for an effective and economic treatment of water effluents containing 2,4-DCP.

Nowadays, various methods have been offered to degrade 2,4-DCP from water such as biodegradation and adsorption. However, bio-treatment is slow and requires control of proper pH and temperature along with the problem of disposal of activated sludge (Martani and Seto, 1991). Moreover, these compounds are highly resistant to bio-treatment. Activated carbon adsorption involves phase transfer of pollutants without decomposition, which induces another pollution problem (Jung et al., 2001). Furthermore, the removals by these techniques are both costly and time consuming. Presently, heterogeneous photocatalysis has been extensively developed as an alternative method due to its ability to destroy a wide range of pollutants. It has been considered as very promising process in water treatment, since it provide high degradation efficiency by the generation of hydroxyl radicals (OH^\cdot) which has powerful oxidation ability. In addition, this technique has a capacity to destroy a wide range of hazardous or recalcitrant pollutants at ambient temperature and pressure, without generation of harmful byproducts.

Heterogeneous photocatalysis is based on the utilization of an oxide semiconductor catalyst activated by the absorption of the light. Over the past decades, TiO₂ is the most commonly used as an effective catalyst. However, many studies have been carried out to evaluate the potential of other catalysts. Among others, ZnO appears to be a suitable alternative to TiO₂, and its photocatalytic mechanism has been proven to be similar to that of TiO₂ (Dindar and Icli, 2001). It has been reported to be more efficient than TiO₂ in some photocatalytic reaction of phenolic compounds like 2-phenylphenol (Khodja et al., 2001). Nevertheless, ZnO can only utilize energy of UV light ($B_g = 3.2$ eV), whereas 46% of the visible spectra of sunlight reaching the surface of earth are unable to be used. Consequently, the use of ZnO under UV light is not feasible and economical.

Accordingly, this study focuses on the modification of ZnO by Fe doping to increase its application in visible light region, and used as catalyst for the removal of 2,4-DCP.

1.2 Objectives

- 1) To prepare Fe-ZnO catalysts by incipient wetness impregnation (IW-IMP) method.
- 2) To investigate physical and chemical characteristics of Fe-ZnO catalysts.
- 3) To examine photocatalytic degradation of aqueous 2,4-dichlorophenol (2,4-DCP) under visible light irradiation.

1.3 Scopes of the study

- 1) Fe-ZnO catalysts are prepared by IW-IMP method using Fe(NO₃)₃•9H₂O with Fe loading 0.5, 2.5, and 5.0 mol% on commercial ZnO nanopowder.
- 2) The prepared catalysts are characterized by various techniques of X-ray diffraction (XRD), BET analysis, UV-Vis diffuse reflectance spectroscopy (UV-DRS), scanning electron microscopy (SEM), X-ray absorption spectroscopy (XAS), and zeta potential analysis.
- 3) The prepared catalysts are used to examine their efficiency in photocatalytic degradation of aqueous 2,4-DCP under visible light using a xenon lamp as the light source.

- 4) The effect of mol% Fe, calcinations temperature, catalysts loading, and initial concentration are our studied parameters.
- 5) 2 mM of potassium persulfate ($K_2S_2O_8$) is added as an oxidant.
- 6) The concentration of 2,4-DCP degradation is measured quantitatively in terms of changes in peak area using a high performance liquid chromatography (HPLC).

1.4 Expected Outcomes

- 1) Understand how to improve effective catalysts for degrading 2,4-DCP under visible light.
- 2) Photocatalysis can be applied to degrade 2,4-DCP and other semi-volatile organic compounds in water.



ศูนย์วิจัยทรัพยากร
จุฬาลงกรณ์มหาวิทยาลัย

CHAPTER II

LITERATURE REVIEW

2.1 2,4-dichlorophenol (2,4-DCP)

2.1.1 Characteristic of 2,4-DCP

2,4-DCP is an organic halogenated compound of cyclic aromatics formed by replacing hydrogen atoms in phenol by two atoms of chlorine. 2,4-DCP is classified as a chlorinated semi-volatile organic compound. It is a hazardous chemical defined by the OSHA hazard communication standard (Dow AgroSciences, 2006 : online). In addition, it is a highly hazardous pesticides identified by Pesticide Action Network of Germany (PAN Germany, 2009 : online). The structure of 2,4-DCP is illustrated in Figure 2.1 (Agency for Toxic Substances and Disease Registry [ATSDR], 1999 : online), and its properties are listed in Table 2.1 (ATSDR, 1999 : online).

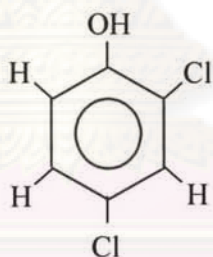


Figure 2.1 Chemical structure of 2,4-DCP.

2,4-DCP is a commercially produced substituted phenol. It mainly used to manufacture agricultural products such as herbicide 2,4-dichlorophenoxyacetic acid (2,4-D) and 2,4-D derivatives (germicides, soil sterilants, etc.), and organochlorine pesticides. It is also reacted with benzene sulfonyl chloride to produce miticides. It is utilized as starting material in the synthesis of higher chlorinated phenols. Moreover, it is used as an intermediate to produce a wood preservative, an antiseptic, and a seed disinfectant (U.S.EPA, 1980 : online).

Table 2.1 Physical and chemical properties of 2,4-DCP.

Property	Information
Molecular formula	C ₆ H ₄ Cl ₂ O
Molecular weight	163 g mol ⁻¹
Appearance	White crystallite solid at room temperature
Odor	Strong medicinal-odor
Meting point	45°C
Boiling point	210°C
Flash point	114°C
Solubility in water at 25°C	4.50 g L ⁻¹
Solubility in organic solvents	Benzene, Carbon tetrachloride, Chloroform, Ethyl alcohol, Ethyl ether
Henry's law constant at 25°C	4.3 x 10 ⁻⁶ atm-m ³ mol ⁻¹
pK _a	7.89
Vapor pressure at 25°C	
• Liquid	0.14 mmHg
• Solid	0.09 mmHg
Partition coefficients	
• Log K _{ow}	3.20
• Log K _{oc}	2.42-3.98

2.1.2 Human exposure and toxicological effects

Because 2,4-DCP is pervasive in the environment, most people are likely to be exposed to 2,4-DCP by inhalation, ingestion, and dermal pathways. Workers are exposed the highest level of 2,4-DCP in workplaces, while the general population can be exposed through their use of products containing 2,4-DCP. Most people are exposed to very low levels of 2,4-DCP in drinking water that has been disinfected with chlorine (chlorinated drinking water). Exposure to 2,4-DCP through contaminated food may result from the production of 2,4-DCP via degradation of herbicide 2,4-D applied to food crops or via ingestion of fish contaminated with some herbicides. Furthermore, oral ingestion of soil can be important among children due to

their hand to mouth activities. Dermal exposure is important if there is a direct contact with contaminated soils and/or water (ATSDR, 1999 : online).

Exposure to 2,4-DCP can cause a variety of health problems ranging from irritation to death. It can react strongly with oxidizing agents and gives off hazardous fumes when heated or in contact with strong acids. Potential symptoms when exposed to 2,4-DCP via inhalation are irritation of the upper respiratory tract, shortness of breath, and labored breathing.

Ingestion of contaminated food and/or drinking water may also cause burns of the mouth and throat, abdominal pain, weakness, tremor, convulsions, and collapse. Laboratory studies carried out with animals showed that 2,4-DCP developed liver and immune system effects. Moreover, high levels given to pregnant female rats in their drinking water caused low birth weight. 2,4-DCP has been reported to have toxic effects on fetuses secondary to maternal toxicities such as decrease in litter size and increase in organ weights, or to have intrinsic fetotoxicities (ATSDR, 1999 : online).

Eye contacts may cause severe irritation with corneal injury, which may result in permanent impairment of vision, even blindness. It is absorbed more readily through skin when in solution or molten than solid. It is classified as corrosive to the skin (Dow AgroSciences, 2006 : online). Skin irritation, skin burn, blister formation, and tissue damage has been observed with skin contact of 2,4-DCP. Furthermore, acute dermal exposure to the heated liquid form of 2,4-DCP resulted in rapid unconsciousness immediately and death has also been reported (Centers for Disease Control and Prevention [CDC], 2000 : online).

International Agency for Research on Cancer (IARC) classifies 2,4-DCP as “*Possible carcinogens (Group 2B)*” (IARC, 1999 : online). This classification is based on limited evidence of carcinogenicity in humans. In addition, it is suspected as a potential endocrine disrupting chemical in lists of EU (The European Commission, 2001 : online).

2.1.3 Environmental contamination

2,4-DCP has been found in the environment as a result of the manufacture, use, and improper disposal of the chemical. 2,4-DCP enter to the atmosphere through volatilization. The major source associated with its production and its use in the manufacture of end-use products. It has been found detected in atmospheric emission from the combustion of municipal solid waste, hazardous waste, coal, wood, and 2,4-DCP-based herbicides. The mean concentration of 2,4-DCP in the air during seven rain events in Portland, Oregon, in 1984 was 1.5 ng L^{-1} (ATSDR, 1999 : online).

The major source of water pollution by 2,4-DCP is industrial waste discharge. It is detected in effluents discharged from industries that manufacture iron and steel, electrical components, pharmaceuticals, and plastics. Small amounts of 2,4-DCP are produced when water is disinfected with chlorine. Other source of 2,4-DCP in aquatic systems include industrial landfill, sewage treatment plant, and drinking water treatment, which can result in the chlorination of phenol. Since 2,4-DCP have greater sorption potential than desorption, they would persist in the aquatic environment for longer periods of time. Unfortunately, the widespread occurrence of DCP in water has been reported in several countries such as water samples from Canada with a concentration $< 0.002\text{-}7.1 \text{ } \mu\text{g L}^{-1}$. It was found in a sample downstream from a chlorinated wastewater discharge in the Netherlands at the maximum level of $0.33 \text{ } \mu\text{g L}^{-1}$. In groundwater samples in Texas found the level of 2,4-DCP in range of $3.2\text{-}79.7 \text{ } \mu\text{g L}^{-1}$ (ATSDR, 1999 : online). It was also detected in range of $< 1.1\text{-}19960 \text{ ng L}^{-1}$ in the surface water of China (Gao et al., 2008).

2,4-DCP is preferentially partition into organic matter due to its $\log K_{ow} > 1$. Release of 2,4-DCP to soil may occur through several process such as landfills, and accidental releases. It is a degradation intermediate of the herbicide 2,4-D and various other pesticides in soil. The use of 2,4-DCP as a wood preservative has also results in the contamination of soil around sawmills. It has been found in soil, at an operating sawmill in Finland, at the level range of $2.7\text{-}47.4 \text{ mg kg}^{-1}$ wet weight (ATSDR, 1999 : online). At a site 2 km distant from a sulphate pulp mill found 2,4-DCP contaminated

in sediments in the Baltic sea at the level of $0.9 \mu\text{g kg}^{-1}$ (UK Marine Special Areas of Conservation [UK Marine SACs], 2001 : online).

There is a report of 2,4-DCP contamination in Thailand. It was detected in the range of $0.02 \mu\text{g L}^{-1}$ in water samples collected from river and seawater in the upper gulf of Thailand (Boonyatumanond et al., 2003 : online).

2.1.4 Standards for 2,4-DCP

International standards applicable to 2,4-DCP are summarized in Table 2.2 (ATSDR, 1999 : online).

Table 2.2 International standards for 2,4-DCP.

Agency	Description	Standard value
<u>Guidelines</u>		
• Water		
U.S.EPA	Ambient water quality criteria	Water & fish: 3.09 mg L^{-1} Fish only: 3.09 mg L^{-1}
U.S.EPA OWRS	Human water quality criteria	$0.3 \mu\text{g L}^{-1}$
U.S.EPA OWD	Health advisories (listed in draft status)	10 kg child: 0.03 mg L^{-1} 70 kg adult: 0.1 mg L^{-1}
• Other		
U.S.EPA	Chronic reference dose (oral)	$0.003 \text{ mg kg}^{-1} \text{ day}^{-1}$
<u>Recommendations</u>		
U.S.EPA	Drinking water	Less than 0.03 mg L^{-1}
U.S.EPA	Surface water	Less than 2.02 mg L^{-1}

Note: U.S.EPA = United States Environmental Protection Agency
 OWD = Office of Drinking Water
 OWRS = Office of Water Regulations and Standards

However, water quality standards for 2,4-DCP content have not been established in Thailand. Only standards for phenolic substances are available which are listed in Table 2.3 (Pollution Control Department [PCD], 2004 : online).

Table 2.3 Thai's standards for 2,4-DCP.

Agency	Description	Standard value
PCD	Drinking water	MAC: 0.002 mg L ⁻¹
	Bottled drinking water quality	MAC: 0.001 mg L ⁻¹
	Industrial effluent	MPV: 1.0 mg L ⁻¹
	Surface water	MAC: 0.005 mg L ⁻¹
	Coastal water	Not more than 0.03 mg L ⁻¹

Note: PCD = Pollution Control Department
 MAC = Maximum Allowable Concentration
 MPV = Maximum Permitted Values

2.1.5 Waste treatment technologies

Various techniques are applied for removing 2,4-DCP such as adsorption and biodegradation. The adsorption of 2,4-DCP onto activated carbon has been studied. The result showed that 2,4-DCP can be adsorbed onto granular activated carbon (Jung et al., 2001). Removal of 2,4-DCP has been performed as well by means of biological activated carbon with the advantage of the biodegradation (Ha and Vinitnantharat, 2000). However, the problem of adsorption method involves the reduction of adsorption capacity due to the existence of background organic matter, and the regeneration of activated carbon is costly and time consuming. In addition, adsorption process is not destructive but only transfers the contaminant from one phase to another phase and does not decompose 2,4-DCP into a harmless substance. Therefore, a new and different kind of pollutant is formed and requires further treatment.

In biodegradation process, microorganism such as bacteria and fungi are used to degrade 2,4-DCP (Martani and Seto, 1991 ; Valli and Gold, 1991). However, the rate of degradation is very low, and difficult to control the condition of microbes. Half-life

of 2,4-DCP in wastewater was found in the level of 125 and 430 hours in aerobic, and anaerobic biodegradation, respectively (ATSDR, 1999 : online). Quan et al., 2004, applied bioaugmentation to a conventional activated sludge system to enhance the degradation of 2,4-DCP. However, bioaugmentation in a biotreatment system does not always work, and the effects of this method have been reported to be less predictable and controllable. Besides, 2,4-DCP can pose severe problems in biological treatment due to its resistance to biodegradation and toxic effects on microbial.

In order to solve the problems of conventional processes, the use of alternative treatment technologies is a matter of great interest. Heterogeneous photocatalysis using light irradiation and catalysts appear to be an attractive option. The main advantage of this method lies in the fact that organic contaminants are mineralized without requiring secondary treatment. Moreover, this method has potential for treating a wide range of hazardous compounds not only from gas phase but also aqueous and solid (soil) phase (Kabra, Chaudhary, and Sawhney, 2004).

Hence, this study is conducted on the heterogeneous photocatalytic decomposition of aqueous 2,4-DCP.

2.2 Heterogeneous photocatalysis

Heterogeneous photocatalysis is one of the advanced oxidation processes (AOPs). The common characteristic of AOPs is the generation of very reactive free radicals, mainly hydroxyl radicals (OH^\bullet) (Litter, 1999). This highly potent and strongly oxidizing radical allows the destruction of organic pollutants with non-selectivity. Furthermore, in this process, organic and inorganic compounds are degraded or transformed into less harmful substances.

2.2.1 Fe-ZnO as a photocatalyst

Heterogeneous photocatalysis involves an acceleration of a photoreaction in the presence of catalysts. The concept of this process is the use of a stable solid catalyst under irradiation for stimulating a reaction at the solid/solution interface. Semiconductors are widely used as catalyst because of the fact that they are low-toxic,

having broad absorption spectra with high absorption coefficients, and their properties can be modified (Chatterjee and Dasgupta, 2005). The most popular catalysts are TiO_2 and ZnO . In the past decade, TiO_2 in the anatase form seems to have the most interesting catalyst. Nevertheless, widespread use of TiO_2 is uneconomic for large-scale in water treatment operations. It is necessary to search for new catalyst that can be potentially better light absorbers. Up to date, ZnO appear to be a suitable alternative to TiO_2 as it has similar band gap energy of about 3.2 eV (Li and Haneda, 2003). It exhibited high reaction and mineralization rates (Poulios, Makri, and Prohaska, 1999). It revealed a better efficiency than TiO_2 in some photoreaction such as TCE (Park and Kang, 1997), reactive dyes (Gouvêa et al., 2000), and azo dye (Daneshvar, Salari, and Khataee, 2004 ; Sakthivel et al., 2003). Moreover, it is suggested as a low cost alternative catalyst for degradation of organics in aqueous solutions (Dindar and Icli, 2001).

ZnO is an II-VI compound semiconductor whose ionicity resides at the borderline between covalent and ionic semiconductor. An excitation binding energy of about 60 meV. The crystal structures shared by ZnO are shown in Figure 2.2 (Özgür et al., 2005). The zinc-blende structure can be stabilized only by growth on cubic substrates, and the rocksalt $[\text{NaCl}]$ structure may be obtained at relatively high pressures. At ambient conditions, the thermodynamically stable phase is hexagonal wurtzite structure in which O atoms are arranged in a hexagonal close-packed type lattice with Zn atoms occupying half the tetrahedral sites (Özgür et al., 2005).

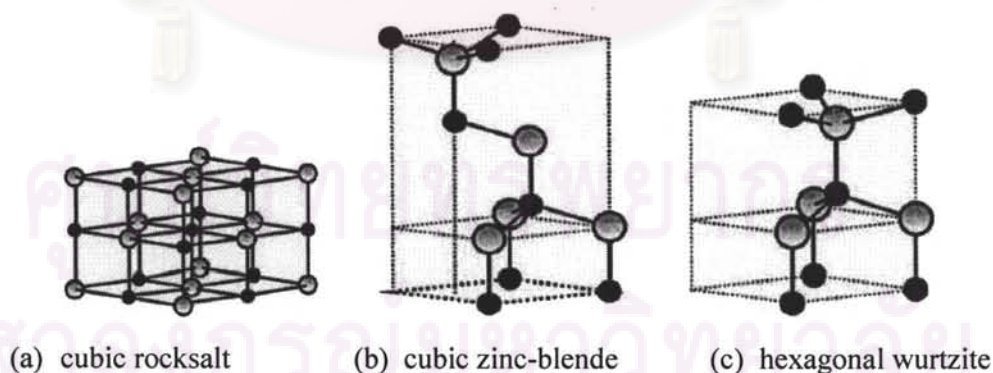


Figure 2.2 ZnO crystal structures. (The shaded gray and black spheres denote Zn and O atoms, respectively.)

Due to its wide band gap energy, the photocatalytic activity of ZnO is limited to irradiation wavelengths in the UV region and can only absorb UV light with wavelength below 400 nm. Unfortunately, the solar spectrum consists only of 3-4% UV light, while 46% and 47% of the spectrum has visible light and infrared radiation. Moreover, some problems still remain in its application such as the fast recombination of photogenerated electron-hole pairs. In order to shift the optical absorption properties of ZnO to the visible region and prevent charge recombination on photocatalyst surface, various attempts have been made such as noble metal deposition (Wang et al., 2004), transition metal doping (Nahar, Hasegawa, and Kagaya, 2006), and non-metallic elements doping (Shifu et al., 2009).

The photodegradation of 2,4-DCP in most of the previous study are experiments under UV light. In this regard, transition metals doping is one of promising method for improving photoactivity of the catalyst from UV to visible region. Many study concluded that Fe-doping TiO_2 can degrade a variety of pollutants in water under visible light. In the study of Nahar et al. (2006), Fe- TiO_2 were prepared by the calcination of Fe_xTiS_2 , and found that the degradation rate of phenol using this catalyst was reactive to the visible light as well as UV light, and more active than TiO_2 P25. The molar ratio of 0.005 was the optimum for both the UV and visible light irradiations. They recommended that modification TiO_2 by doping Fe can observed the red shift in the UV-Vis spectra due to the introduction of the 3d electron state of Fe^{3+} , $3d^5$, in the conduction band of TiO_2 . Fe- TiO_2 was also prepared by a one-step flame spray pyrolysis technique in the research of Teoh et al., 2007. They found that under visible light irradiation, the rate of oxalic acid mineralization by 1.0 g L^{-1} of Fe- TiO_2 (Fe/Ti = 0.05) was 6.4 times higher than that of similarly prepared bare TiO_2 and TiO_2 P25. Fe- TiO_2 also prepared in the experiment of Zhang and Lei (2008) by metal organic chemical vapor deposition method. The catalyst showed a slight shift to longer wavelengths and stronger absorption in the visible region, compared to the non-doped catalyst. Moreover, the catalyst exhibited good photoactivities for the degradation of methyl orange azo dye wastewater under visible light irradiation. The activity of catalysts was evaluated by calculating the pseudo first order kinetic constants (k). From the calculation, they found that undoped TiO_2 display very poor

catalytic performance under visible light ($k = 0.006$), while k was significantly improved after Fe doping.

Since ZnO have similar properties to TiO_2 , Fe-doping may be improve the photoactivity of ZnO same as TiO_2 . Many studies analyzed the properties of Fe-ZnO catalysts but did not investigate their efficiency in photocatalytic reaction. In the study of Wang, Thomas, and O'Brien (2006) suggested that doping ZnO with Fe produces a blue shift proportional to the concentration of Fe ions. They recommended that the increase in the absorption in the region of 2.9-3.2 eV is due to the d-d transition of Fe ions. Baek, Song, and Lim (2007) accomplished that Fe doping improved the optical property of ZnO nanorod due to the reduction of oxygen deficiencies. They also recommended that addition of Fe^{3+} into ZnO structure disturbs the recombination of e^-h^+ by bonding with e^- in singly ionized oxygen vacancies. At the present time, Sharma et al. (2009) synthesize Fe-doped ZnO by co-precipitation method. They found that the mean sizes of the catalysts are 3-10 nm. Furthermore, they suggested that the hexagonal wurtzite structure of ZnO gradually degrades with increasing Fe doping content. Zhang et al. (2009) fabricate Fe-doped ZnO by sol-gel method and found that when Fe ions increased, the blue emission was observed around 427 nm.

Several methods were applied to prepared catalysts such as sol-gel, co-precipitation and impregnation. Among them, impregnation method has several advantages, including simpler synthesis, fewer steps, lack of a filtration step, and shorter synthesis time. Thus, this method appears more attractive for industrial applications.

Kim and Ahn (2009) explained that impregnation (IMP) method is a technique in which a solution of the precursor is brought in contact with the support. Two methodologies exist, i.e. conventional IMP method and incipient wetness IMP (IW-IMP) method. In conventional IMP method, the support is dipped into an excess quantity of solution containing the precursor. In IW-IMP method, also referred to as "pore volume impregnation", just enough solution of the precursors is used to fill the

pore volume of the support. Roggenbuck, Waitz, and Tiemann (2008) described that the purpose of IW-IMP method is the solution is entirely drawn into the pores by capillary forces and no precursor material is deposited on the outer surface of the support. In addition, they also found that IW-IMP method is more efficient than conventional IMP method.

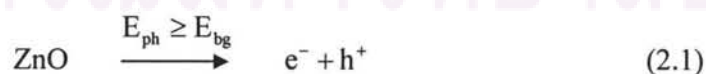
Navío et al. (1998) investigated the efficiency of two different precursors i.e. $\text{Fe}(\text{NO}_3)_3 \cdot 9\text{H}_2\text{O}$ and Fe(III) acetylacetonate in the preparation of Fe-TiO₂ catalyst by the impregnation method. They found that samples prepared from $\text{Fe}(\text{NO}_3)_3 \cdot 9\text{H}_2\text{O}$ containing low amounts of Fe (< 2 wt.%) were more efficient for nitrite oxidation than pure TiO₂ catalyst, whereas Fe(III) acetylacetonate were less active than pure TiO₂.

Therefore, this work is focused on the preparation of Fe-ZnO catalysts by IW-IMP method and $\text{Fe}(\text{NO}_3)_3 \cdot 9\text{H}_2\text{O}$ is selected as a precursor.

2.2.2 Photocatalytic reaction

In photocatalytic reaction, ZnO semiconductor catalyst exhibit a void energy region in which no energy levels are available to promote the recombination of an electron and hole produced by photoactivation in the solid. The void region that extends from the top of the filled valence band (VB) to the bottom of the vacant conduction band (CB) is called the band gap (Kabra et al., 2004).

The reaction is initiated when ZnO catalyst is illuminated with photons (E_{ph}) whose energy equal to or greater than their band gap energy (E_{bg}), resulting in molecular excitation. This molecular excitation results in the generation of mobile electron (e^-) in the higher energy conduction band (E_{CB}) and positive hole (h^+) in the lower energy valence band (E_{VB}) of the catalyst, according to equation 2.1 and the reaction illustrated in Figure 2.3 (Chatterjee and Dasgupta, 2005).



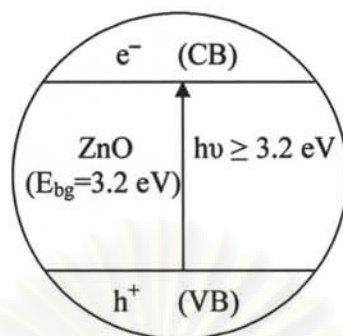


Figure 2.3 The e^-h^+ generation in ZnO particle.

Unfortunately, there is a competing e^- and e^-h^+ recombination step (the reverse of equation (2.1)), and this result in process inefficiencies and the waste of the energy supplied by the photon. The e^-h^+ recombination can be considered as one of the major factors limiting the efficiency of the photo-reaction. The schematic of e^-h^+ recombination is shown in Figure 2.4 (Chatterjee and Dasgupta, 2005).

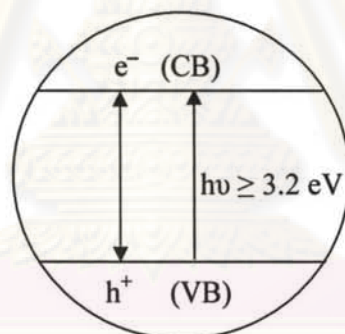
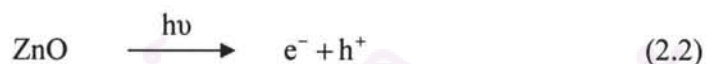


Figure 2.4 The e^-h^+ recombination process.

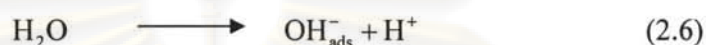
The photocatalytic reaction can be represented as a number of mechanistic steps. The first step is a photo-excited ZnO generates the e^-h^+ pairs.



The second step is electron transfer from the adsorbed substrate (RX_{ads}), adsorbed water or the OH_{ads} ion, to the electron hole.



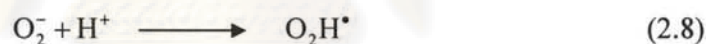
The third step is of great importance, mostly because of the high concentrations of OH^- , given water dissociation into ions.



Molecular oxygen acts as an acceptor species in the electron-transfer reaction.



Super-oxide anions (O_2^-) in equation (2.7), can subsequently be involved in the following reactions.



Photoconversion of hydrogen peroxide gives more OH^\bullet free radical groups.



Finally, OH^\bullet radicals oxidize organic adsorbed pollutants (RX_{ads}) onto the surface of the ZnO particles.



The OH^\bullet radicals, as described by equation (2.11), are very reactive and attack the pollutant molecule to degrade it into mineral acids including CO_2 and H_2O (De Lasa, Serrano, and Salaices, 2005). The photocatalytic mechanism illustrated in Figure 2.5 (Daneshvar et al., 2004).

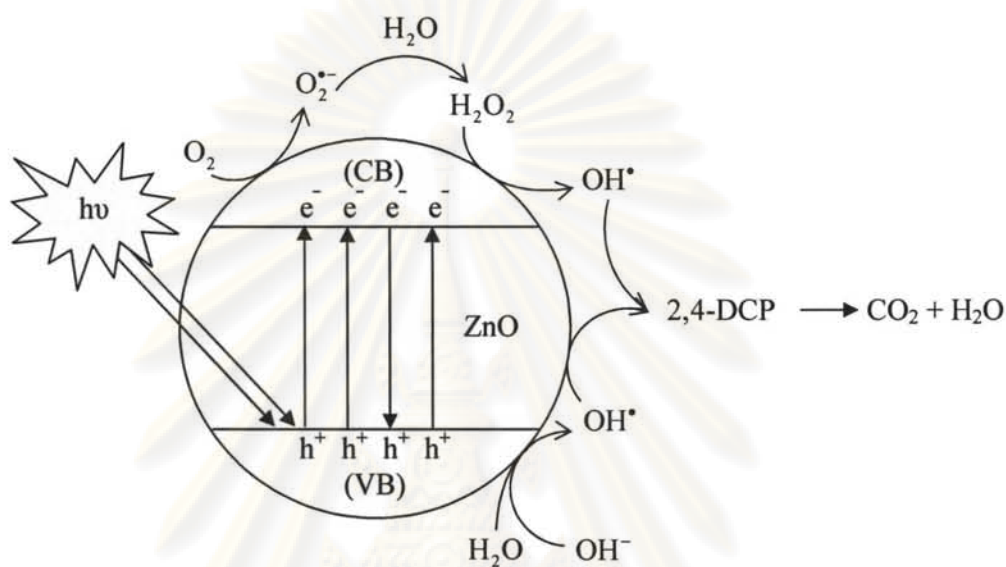
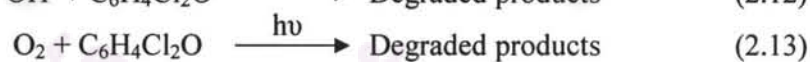


Figure 2.5 General mechanism of photocatalysis.

In case of 2,4-DCP, the generally chemical reaction for 2,4-DCP photocatalytic oxidation is given as (Xiangzhong, Wei, and Jincai, 2002):

Oxidation reaction



Reduction reaction



2.2.3 Photocatalysis of phenolic compounds

Many researchers prove that heterogeneous photocatalysis can degrade effectively phenolic compound and can be useful technique for the treatment of wastewater. In the study of Rao et al. (2003), TiO_2 P25 was used to the

photodegradation of 2-chlorophenol (2-CP) under UV light. In this work, the reactor maintained at 35°C, and a 400 W medium pressure mercury vapor lamp ($\lambda=365$ nm) was used. The results found that approximately 95% of 2-CP (100 mg L⁻¹) was removed in 2 h at pH 5 by adding 0.2 g L⁻¹ of TiO₂.

The photo-oxidation of phenol and chlorophenols were studied in the research of Lathasree et al., 2004. In this work, a 6 W low pressure mercury lamp ($\lambda=253.7$ nm) was used for irradiating the test solution. The results show that in the presence of UV light and ZnO, phenol was completely mineralized to CO₂, H₂O and Cl⁻ within an hour. The degradation rate of chlorophenols increased with increase the weight of ZnO up to an optimal loading 2.0 g L⁻¹. They also found that the degradation rate of phenol was favorable in the neutral pH, while chlorophenols undergo faster degradation rate at lower pH. The degradation rate was also studied over a concentration of phenols range of 40-100 mg L⁻¹. The results exhibited that the degradation rate were high at lower concentration and it decreased with increase in concentration. Moreover, they suggested that ZnO is quite stable and photocorrosion after the fifth cycle of reuse. In the same year, Salah et al. (2004) studied the photodegradation of phenol using ZnO and three commercial TiO₂ (Degussa P25, TiO₂-A1, and TiO₂-A2). The experiment carried out at 25°C, and 125 W medium pressure mercury lamp ($\lambda=300$ nm) was used. After 5 h irradiation, they found that the rate of removal greater for ZnO (99.75%) and Degussa P25 (92%) than TiO₂-A1 (73%), and TiO₂-A2 (60.67%).

Bayarri et al. (2005) studied the photocatalytic treatment of 2,4-DCP by using TiO₂ in suspension as catalyst and a 1500 W Xenon lamp ($\lambda=300-436$ nm) as a source of irradiation. The results show that in 6 hours of treatment with 2.0 g L⁻¹ of TiO₂ loaded, more than 99% of 2,4-DCP (125 mg L⁻¹) was degraded and a mineralization up to 80% was achieved. In addition, the best degradation rate was found at pH 5.6.

The photodegradation of phenol in aqueous ZnO suspension was also studied in the research of Pardeshi and Patil, 2008. The activity of ZnO is compared between 2 light source that are sunlight (approximately 4% UV and 43% visible light, between

8:00 AM and 5:00 PM in December-February) and artificial visible light (1000 W Xenon lamp, $\lambda=420$ nm). The results show that under sunlight and ZnO, phenolic solutions at 25-75 mg L⁻¹ were completely mineralized to CO₂ and H₂O within 8 hours, while only 47% degradation were observed under visible light, The optimum loading of ZnO was 250 mg 100 mL⁻¹. They recommended that photodegradation of phenol was favorable in weakly acidic or neutral pH. Moreover, they found that ZnO can be reused for five times.

Kansal, Singh, and Sud (2009) investigated the photodegradation of 2,4-DCP under UV light using TiO₂ Degussa P25 and sodium hypochlorite as an oxidant. For the degradation experiments, the initial concentration of 2,4-DCP was 100 mg L⁻¹, 5 tube of 30 W UV lamp ($\lambda=365$ nm) were used, and irradiation time is 5 h. The results show that 20% degradation was achieved due to adsorption on TiO₂ and only 15% degradation was achieved when irradiated under UV light alone. However, the degradation under UV and TiO₂ was found to be 45% and up to 75% if adding oxidant at the optimal concentration is 10.32×10^{-6} M. They also concluded that the degradation rate tends to increase with increase TiO₂ dose and reaches maximum at 1.1 g L⁻¹. Moreover, they suggested that the maximum degradation has been obtained in the pH range of 4-4.5.

Photodegradation of phenol under UV by using TiO₂ as catalyst was observed in the experiment of Naeem and Ouyang, 2009. The most appropriate conditions for degradation 3.56×10^{-4} mol L⁻¹ of phenol at 25°C were pH 5, 0.2 g L⁻¹ TiO₂. They found that the presence of oxidants such as BrO₃⁻, H₂O₂ and S₂O₈²⁻ enhance the degradation efficiency appreciably.

Up to date, there are a few reports on photodegradation of 2,4-DCP using Fe-ZnO as catalysts. Therefore in this study, Fe-ZnO catalysts prepared by IW-IMP method are utilized for removing aqueous 2,4-DCP under visible light irradiation.

CHAPTER III

MATERIAL AND METHODS

3.1 Catalyst preparation

3.1.1 Materials

- Zinc oxide nanopowder: ZnO (>99.7%, Inframat[®] Advanced Materials)
- Ferric nitrate nonahydrate: $\text{Fe}(\text{NO}_3)_3 \cdot 9\text{H}_2\text{O}$ (99%, Merck)
- Deionized water: DI

3.1.2 Preparation procedures

In this study, the catalyst preparation by IW-IMP method was applied following the procedure of Nahar et al., 2006. First, $\text{Fe}(\text{NO}_3)_3 \cdot 9\text{H}_2\text{O}$ corresponding to 0.5, 2.5, and 5.0 mol% of Fe in commercial ZnO nanopowder were weighed, and dissolved in 1.3 mL DI water. Second, the solutions were gradually dropped onto ZnO nanopowder. The material should be sonicated and kept for 30 min. After the impregnation process, the catalysts were dried at 70°C for 36 h and ground with an agate mortar. Finally, the catalysts were calcined in air at temperatures of 400, 550, and 700°C with heating rate 2°C min⁻¹ for 3 h. The schematic diagram of the catalyst preparation is show in Figure 3.1.

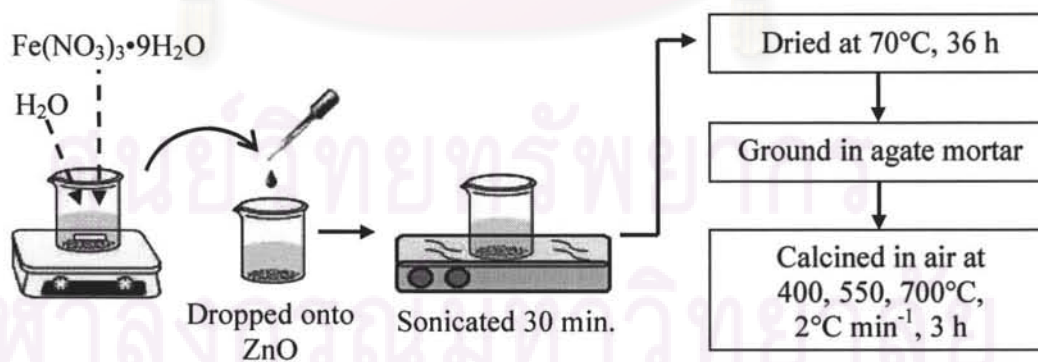


Figure 3.1 A diagram of Fe-ZnO samples prepared by IW-IMP technique.

3.2 Catalyst characterizations

3.2.1 X-ray diffraction (XRD)

XRD was used to identify the crystallographic phase that is present in the catalyst. It was commonly used to identify unknown samples by comparing diffraction data with standards in the International Centre for Diffraction Data (JCPDS file).

In this study, XRD measurement was performed at room temperature using X-ray diffractometer (Bruker-8) with Cu K α wavelength ($\lambda = 0.15406$ nm). The sample was scanned in the 2θ range from 20° - 80° . The accelerating voltage and emission current were 40 kV and 40 mA, respectively. The crystallite sizes (D) can be estimated using Scherrer equation (Tayade, Kulkarni, and Jasra, 2006):

$$D = \frac{k\lambda}{\beta \cos\theta} \quad (3.1)$$

where: D = the crystallite sizes (nm)
 k = the Scherrer constant (0.90)
 λ = the wavelength (0.15406 nm)
 θ = the Bragg's angle (degree)
 β = the full-width at the half-maximum (FWHM) of the peak (degree)

3.2.2 Brunauer-Emmett-Teller (BET) method

The isotherm and surface area were obtained by the most common adsorbate, N₂, at -196°C on a Quantachrome instruments (AUTOSORB-1) sorption analyzer where nitrogen adsorption and desorption isotherms were measured. Prior to the measurement, each sample was first degassed at 250°C for 2 h to remove the moisture. Furthermore, specific surface areas of the samples were calculated from the adsorption data by using the standard BET method.

3.2.3 Scanning electron microscopy (SEM)

SEM was used for inspecting morphologies of the sample. Powder sample was scattered on an adhesive tape on a brass bar. SEM micrograph was conducted on JEOL (JSM-6400) scanning microscope. The sample was then coated with gold and transferred into the sample chamber. The accelerating voltage was operated at 15 kV. The SEM images were print out using the video graphic printer (UP-897MD, Sony).

3.2.4 UV-Vis diffuse reflectance spectroscopy (UV-DRS)

The absorption properties of the sample were investigated on UV-Vis diffuse reflectance spectroscopy (Hitachi U-3501), using BaSO₄ as a reflectance standard. The optical spectra of the sample were evaluated at room temperature in the wavelength range from 300-800 nm. The light sources used were deuterium lamp and halogen lamp. In addition, the indirect band gap energy (E_g) of each sample can be calculated by fitting the absorption data to the direct transition equation (Murphy, 2007):

$$k\alpha\nu = A (\alpha\nu - E_g)^2 \quad (3.2)$$

where: k = the optical absorption coefficient
 $\alpha\nu$ = the photon energy (eV)
 A = the constant
 E_g = the energy band gap (eV)

3.2.5 X-ray absorption spectroscopy (XAS)

X-ray absorption spectroscopy was performed in absorption near edge structure (XANES) mode. It might easily be the most popular technique for determining oxidation states of the catalyst. The XANES spectra can be used as a fingerprint technique, provided by available spectra of reference compounds.

This experiment was performed at Beamline-8 of Synchrotron Light Research Institute (Public organization), Thailand. The XANES spectra of Fe-ZnO samples and reference compounds (FeO, Fe₂O₃) were measured in the energy region of the Fe K-

edge (7112 eV) in Fluorescence mode using Ge detector. The X-rays were operating at 1.2 GeV and diffracted with a Si(111) two-crystal monochromator. The XANES spectra were normalized with the Athena program, the edge shifts were corrected to standard reference compounds to determine characteristics of the sample.

3.2.6 Zeta potential analysis

Zeta potential is derived from measuring the mobility distribution of a dispersion of charged particles as they are subjected to an electric field. It widely used for quantification of the magnitude of the surface charge at the double layer (Chang and Tsai, 2008).

In this work, Zeta potential values of catalysts were measured by a zeta meter (Zeta meter system 3.0+, Meditop Co., Ltd.). Before such measurements, 0.5 mg catalysts were suspended in 20 mL of a solution. The pH of the suspension was adjusted to a given value employing HNO₃ or NaOH. An average of at least 5 measurements for each sample was reported.

3.3 Photocatalytic experiment

3.3.1 Materials

- 2,4-dichlorophenol: 2,4-DCP (99%, Acros Organics)
- Potassium persulfate: K₂S₂O₈ (99%, Carlo Erba)
- Nitric acid: HNO₃ (69-70%, JT Baker)
- Sodium hydroxide: NaOH (99%, Merck)
- Methanol: CH₃OH (99.9% HPLC, RCI Labscan)
- Acetonitrile: CH₃CN (99.9% HPLC, RCI Labscan)
- Water: H₂O (HPLC, RCI Labscan)
- Deionized water

3.3.2 Photoreactor setup

This experiment was set up in a batch photoreactor of 250 mL in volume. The light source was a 1500 W Xenon lamp (light intensity: 500 W m²) and cutoff at

400 nm by 1 M sodium nitrite (NaNO_2) to control the wavelength and to ensure illumination by visible light source only. A magnetic stirrer was located at the photoreactor's base to ensure homogeneous mixing of the solution throughout the reaction. A cooling water system was also used to control the reaction temperature at 25°C . The photoreactor was wrapped with aluminium foil in order to minimize escaped radiation due to transmission from photoreactor walls. The photoreactor setup is illustrated in Figure 3.2.

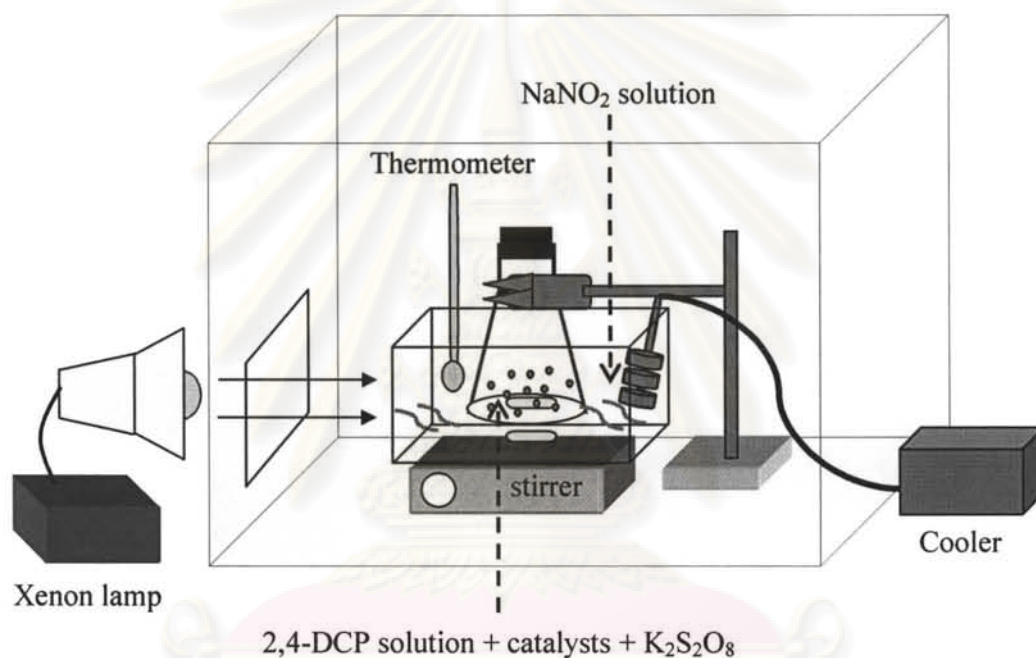


Figure 3.2 Schematic diagram of the photoreactor.

3.3.3 Photocatalytic procedures

Aqueous solutions containing different concentration of 2,4-DCP were prepared by dissolving pure 2,4-DCP in DI water. After that, Fe-ZnO catalysts were dispersed into 2,4-DCP solution. The initial pH of the solution was adjusted to 8.5 with HNO_3 and NaOH , and measured with pH meter (Ultrabasic pH meter, Denver instrument). The suspension was stirred in the dark for 60 min, and then 2 mM $\text{K}_2\text{S}_2\text{O}_8$ was added. After that, the lamp was switched on to initial the reaction. 1.5 mL

of the sample was withdrawn from the reactor at different reaction times. The blank test was also carried out by irradiating 2,4-DCP solution without the catalyst under visible light irradiation for checking the photo-induced self-sensitized degradation.

3.3.4 Analytical method

The 2,4-DCP concentration in each degraded sample was analyzed using the high performance liquid chromatography with diode-array detector (HPLC-DAD 1200 series detector, 1100 series pump and controller, Agilent technologies). The UV detector was set at 280 nm for the maximum absorption of 2,4-DCP. The column was Hypersil C18 ODS (125 x 4 mm I.D, 5 μm column). The mobile phase was a mixture of 60% methanol and 40% water with flow rate of 1.0 mL min^{-1} . The mobile phase was filtered and degassed for 30 min prior to use. Before analysis, the sample was filtered with 0.45 μm syringe filter PTFE to remove all solid particles.

3.3.5 Experimental design and statistical analysis

Response Surface Methodology (RSM) is an empirical model used to evaluate the relationship between a set of controllable experimental factors and observed results (Bezerra et al., 2008). By using RSM analysis, it is able to determine whether factor is significant by referring to the '*p*-value' based on the analysis result. To determine whether the factor is affecting the degradation percentage of 2,4-DCP, the '*p*-value' should be less than 0.5.

In this study, we adopted RSM experiments based on a Box-Behnken design (BBD) with a quadratic model in order to find out the optimal operating conditions for the next laboratory work. The experimental data were analyzed statistically using Minitab[®] 15 software (Minitab Inc.). The analysis can be used to reduce amount of experiment to be done. Three parameters (mol% Fe, calcinations temperatures, and catalyst loading) were chosen for studying the effect of individual factors and the effects of interactions of studied factors. The chosen levels for each parameter were showed in Table 3.1. The number of experiments required is given by:

$$N = 2k(k-1) + C_0 \quad (3.3)$$

where: N = the number of experiments
 k = the number of parameters
 C₀ = the number of center points

For three parameters (n=3) with three central points and two replicates, the total number of experiments in this study were 30. The experiments were performed in a random manner in order to avoid any systematic bias in the outcomes.

Table 3.1 The range and level of independent parameters.

No.	Parameter	Unit	Range and level of actual value		
			-1	0	+1
1	Fe contents	mol%	0.5	2.5	5.0
2	Calcinations temperature	°C	400	550	700
3	Catalyst loading	g L ⁻¹	0.5	1.25	2.0

ศูนย์วิทยทรัพยากร
 จุฬาลงกรณ์มหาวิทยาลัย

CHAPTER IV

RESULTS AND DISCUSSION

4.1 Catalyst characterizations

4.1.1 Structure and crystallite size

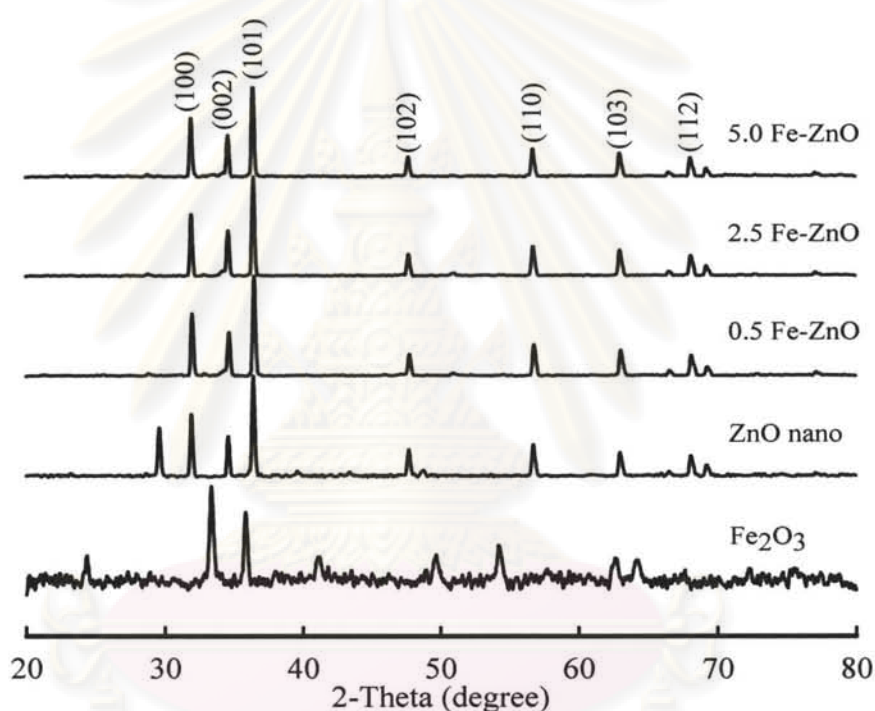


Figure 4.1 XRD patterns of bare ZnO and Fe-ZnO samples at different mol% Fe calcined at 700°C, compared with a standard Fe₂O₃.

Effects of Fe content and calcination temperature on the structure of ZnO nanopowder are shown in Figure 4.1 and 4.2, respectively. The XRD patterns of the prepared samples were compared with bare ZnO as well as Fe₂O₃. As shown in the Figure 4.1 and 4.2, all samples exhibit the characteristic peaks of hexagonal wurtzite ZnO at (100), (002), (101), (102), (110), (103) and (112) planes which corresponds to

the standard JCPDS file no.36-1451 (Sharma et al., 2009). In addition, the content of Fe might be too small to determine its existence, which possibly indicated that Fe was well dispersed onto the surface of ZnO nanopowder.

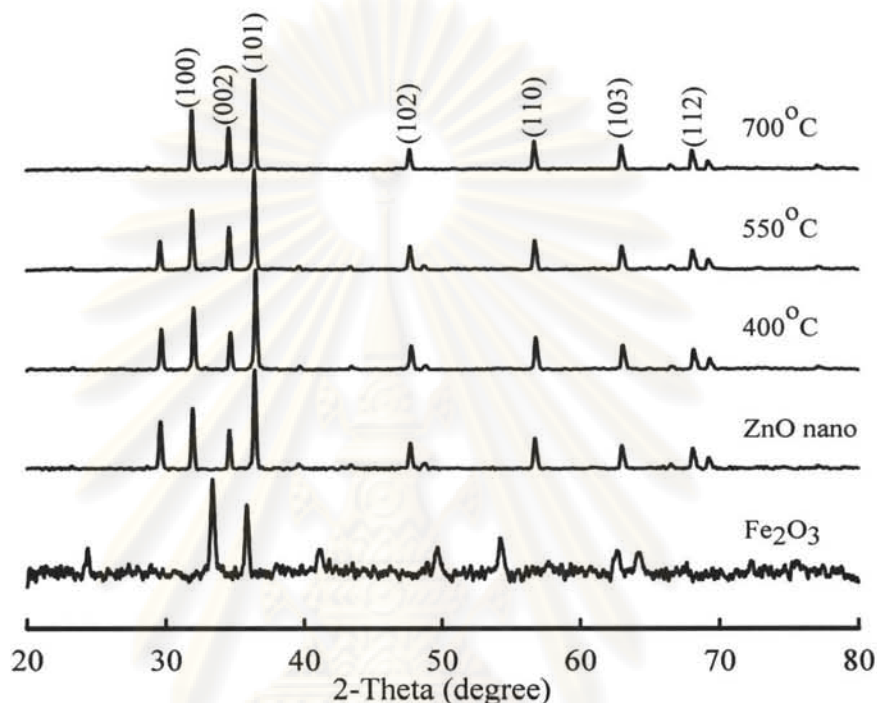


Figure 4.2 XRD patterns of bare ZnO and 5.0 mol% Fe-ZnO samples at different calcination temperatures.

The diffraction peaks at 2θ around 29.5° can be observed in bare ZnO nanopowder, and the doped sample calcined at 400 and 550°C . This peak might be indicated to (111) plane of ZnS which corresponds to cubic zinc blend structure (Bera and Basak, 2010 ; Lü et al., 2007 ; Porambo, Howard, and Marsh, 2010), or (002) plane of $\text{Zn}_x\text{Sr}_x\text{S}$ in rocksalt structure (Chen et al., 2004), which was possibly contaminated during the production of ZnO. This peak was also gradually decreased with increasing calcination temperature (Figure 4.2). The possible reason is that high temperature can eliminate the contaminants from the structure to form pure ZnO nanopowder. It can be inferred that both cubic zinc blend structure and rocksalt structure have been transformed into wurtzite phase of ZnO.

The crystal sizes were also determined by XRD analysis using Scherrer equation and FWHM of (101) peak representing wurtzite ZnO was selected to calculate. The results are defined in Table 4.1. For the sample doped with different Fe and calcined at 700°C, the average crystal sizes around 37.63 nm which was slightly increased compared to bare ZnO. As well as 5.0 mol% Fe doping one, the average crystal sizes (37.14 nm) was somewhat bigger than that of bare ZnO. However, there is not significant by the size.

Table 4.1 Crystal sizes and surface areas of bare ZnO, and Fe-ZnO samples.

Sample	Calcination temperature (°C)	Crystal size (nm)	BET surface area (m ² g ⁻¹)
ZnO nanopowder	-	35.93	4.48
0.5 Fe-ZnO	700	37.58	4.90
2.5 Fe-ZnO	700	37.58	4.98
5.0 Fe-ZnO	700	37.74	5.52
5.0 Fe-ZnO	550	37.74	7.39
5.0 Fe-ZnO	400	35.95	7.75

4.1.2 BET surface area

Table 4.1 shows the specific surface area (S_{BET}) of the samples prepared at different Fe doping concentration and different calcination temperature. It can be seen from table 4.1 that all doped samples had higher S_{BET} than bare ZnO. The S_{BET} of the samples doped with Fe at 0.5, 2.5 and 5.0 mol% slightly increase from 4.90, 4.98, and 5.52 m² g⁻¹, respectively. It can deduce that the S_{BET} increases along with increasing the dopant concentration. Moreover, the results showed that the sample calcined at 400, 550, and 700°C provided S_{BET} of 7.75, 7.39, and 5.52 m² g⁻¹, respectively. The calcination temperature also showed the effect on the S_{BET} . With increasing calcination temperature, the S_{BET} evidently decreases, probably due to the fact that high temperature and long calcination time for 3 h cause particle aggregation and sintering.

4.1.3 Surface morphology

The SEM images demonstrate the surface morphology of the samples, shown in Figure 4.3. Surface morphology of all doped samples is nearly rectangular chunk shape as bare ZnO nanopowder. An agglomeration of the samples could not be occurred obviously, and the surface morphology of doped samples was not generally different from bare ZnO. This implied that the surface morphology of our samples was not affected by both doping Fe amount and increasing calcination temperature.

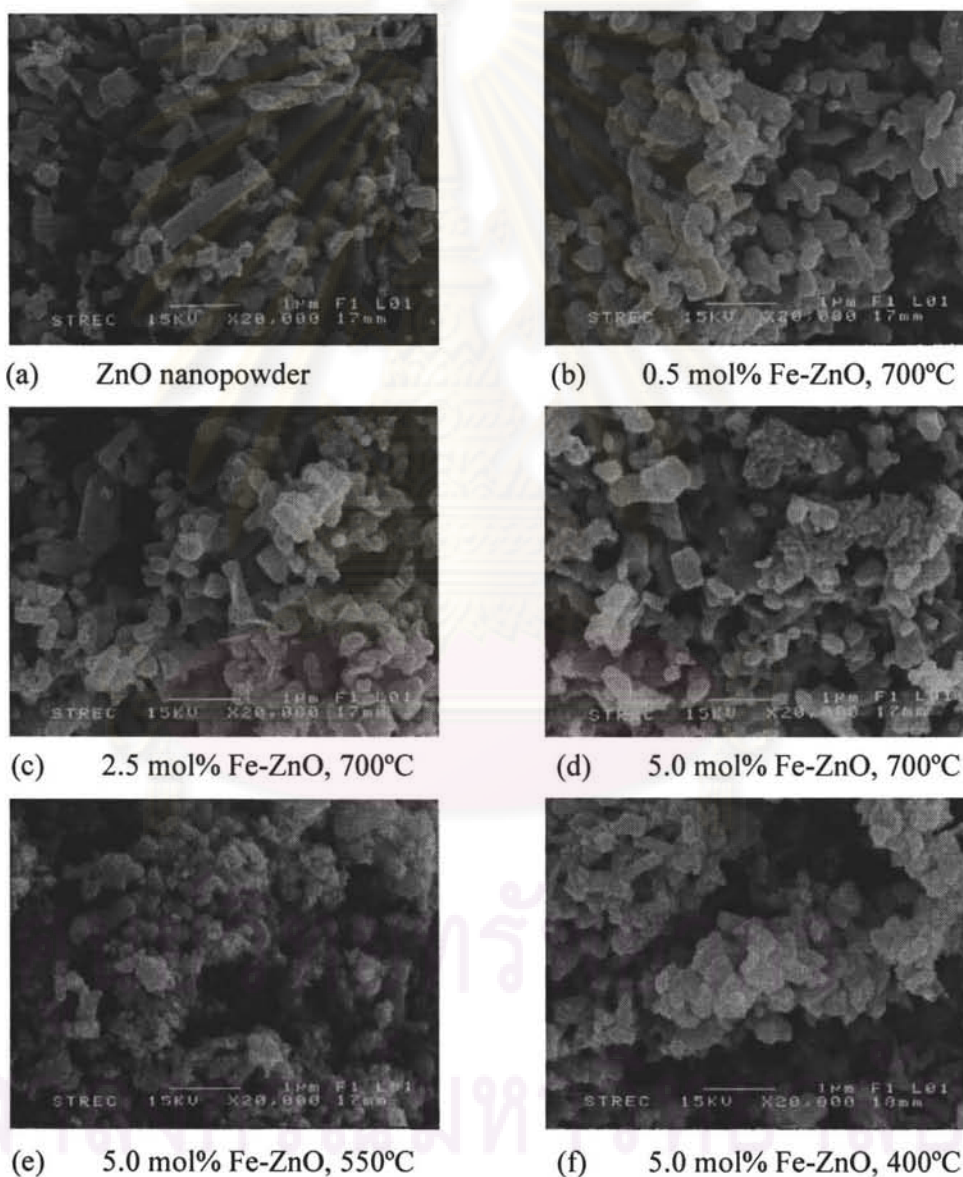


Figure 4.3 SEM images of the bare ZnO and doped samples (20kX).

4.1.4 Optical absorption property

Commonly, metal ions doping obviously affects the light absorption characteristics of ZnO. Figure 4.4 and 4.5 show the UV-DRS spectra of Fe-ZnO prepared at different Fe contents and the spectra of 5.0 mol% Fe-ZnO calcined at different temperatures, respectively. As shown in the figures, the spectra of bare ZnO shows no absorption in visible region (400-800 nm). A significant increase in the absorption at wavelengths shorter than 400 nm can be assigned to the intrinsic band gap absorption of ZnO (3.2 eV). Figure 4.4 reveals that the samples doped with different Fe contents display stronger absorption in the visible zone. The light absorption increases with increasing the dopant amount of Fe, accompanied by the color of the samples changing from creamy to brown. In addition, it can be deduced from Figure 4.5 that 5.0 mol% Fe calcined at 700°C presents a higher powerful absorption in the visible range.

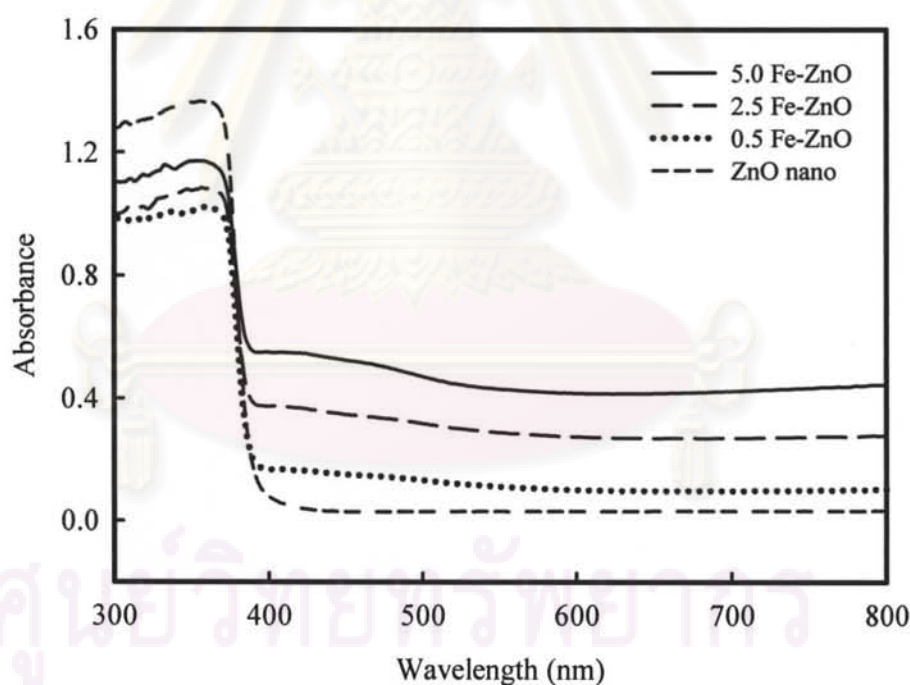


Figure 4.4 UV-DRS spectra of bare ZnO and Fe-ZnO samples at different Fe contents, calcined at 700°C.

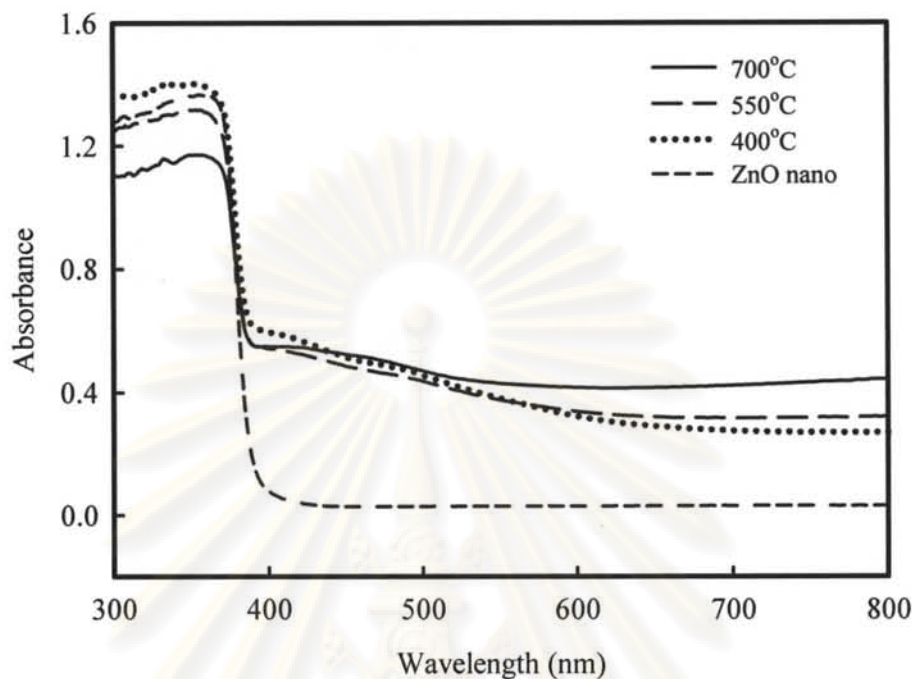


Figure 4.5 UV-DRS spectra of bare ZnO and 5.0 mol% Fe-ZnO samples at different calcination temperatures.

The band gap energy (E_g) for all samples was determined by fitting the absorption data to the transition equation 3.2. Figure 4.6 and 4.7 are shown the graph of $(k\alpha\nu)^{1/2}$ versus photon energy ($h\nu$) which referred to as the Tauc plots for all samples. The linear portion of the curve when extrapolating to zero gives the value of the E_g . According to the Tauc plots, the E_g of doped samples were about 3.11 eV as well as the E_g of bare ZnO. The E_g of the samples in our study are closed to the value of ZnO reported in literature (Meansiri, Laokul, and Promarak, 2006). In addition, we also found that both Fe doping, and calcination temperatures do not affect on the E_g of the samples. However, visible light absorption can be observed in doped samples because Fe^{3+} might act as e^- transfer from $ZnO_{(VB)}$ to $Fe_2O_{3(VB)}$.

จุฬาลงกรณ์มหาวิทยาลัย

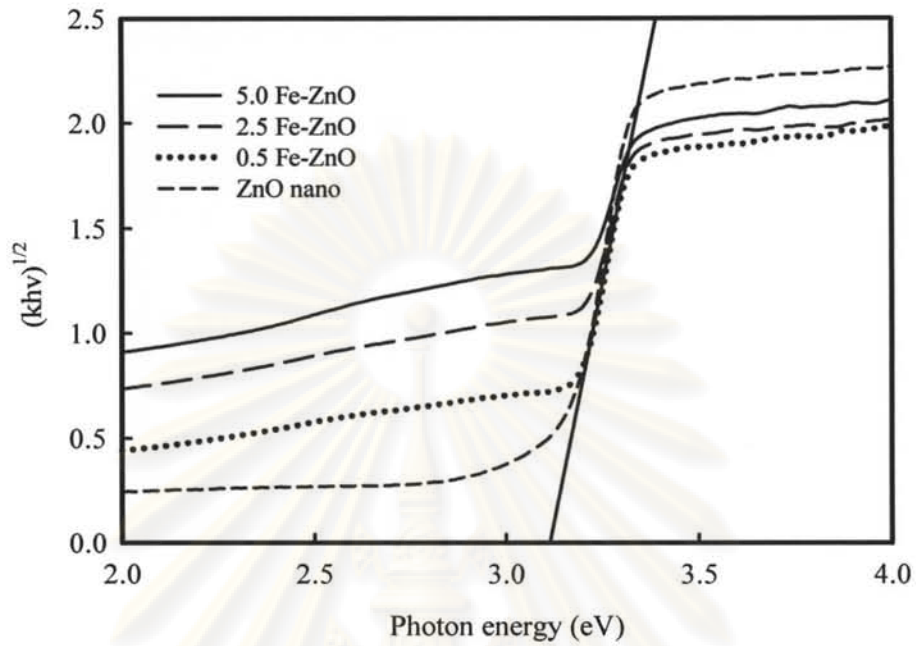


Figure 4.6 Tauc plots of bare ZnO and Fe-ZnO samples at different Fe contents, calcined at 700°C.

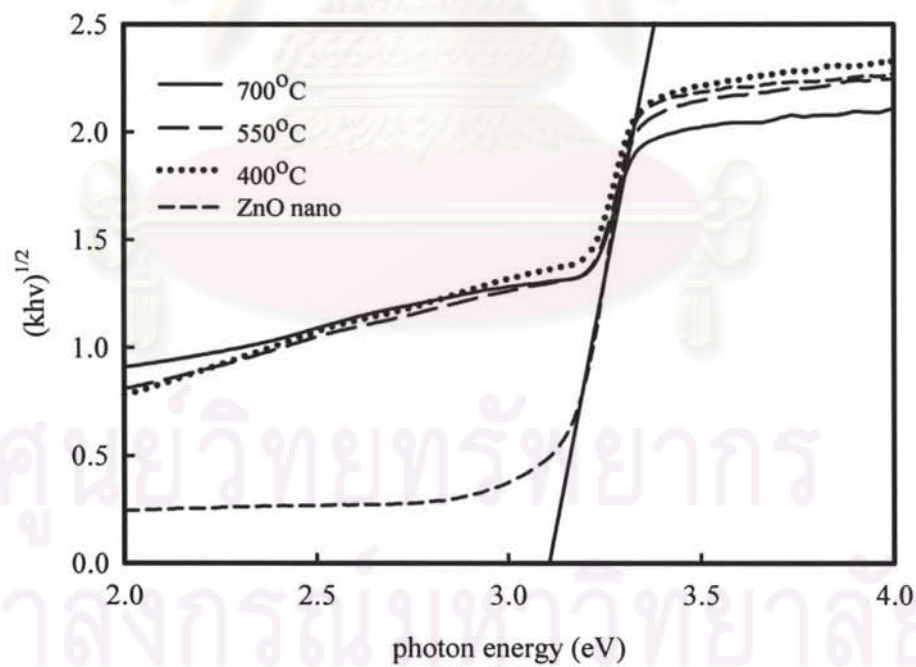


Figure 4.7 Tauc plots of bare ZnO and 5.0 mol% Fe-ZnO samples at different calcination temperatures.

4.1.5 Oxidation state

XANES analysis was used to identify directly the Fe oxidation state in the sample. In XANES, the oxidation state of metal cation can be concluded from the energy shift of the pre-edge absorption features. Pre-edge is a small peak before the sharp rise in the spectrum. It is resulted from of the excitation of the core electron of Fe to empty bound states.

Figure 4.8 and 4.9 show that the spectra of doped samples demonstrate a pre-edge peak around 7115.81 eV, which similar to the pre-edge peak of Fe_2O_3 . The spectrum can be attributed to the $1s \rightarrow 3d$ electronic transition in Fe. The results confirmed that Fe in our samples was a trivalent state, a characteristic of octahedral symmetry. However, the shape of the spectra corresponding to Fe_2O_3 was not different on both studied factors. According to crystal field theory, Fe^{3+} is relatively stable as compared to Fe^{2+} due to its half-filled d orbital (d^5) (Naeem and Ouyang, 2010). Hence, the XANES result inferred that Fe-ZnO samples in this study were suitable for photodegradation of 2,4-DCP.

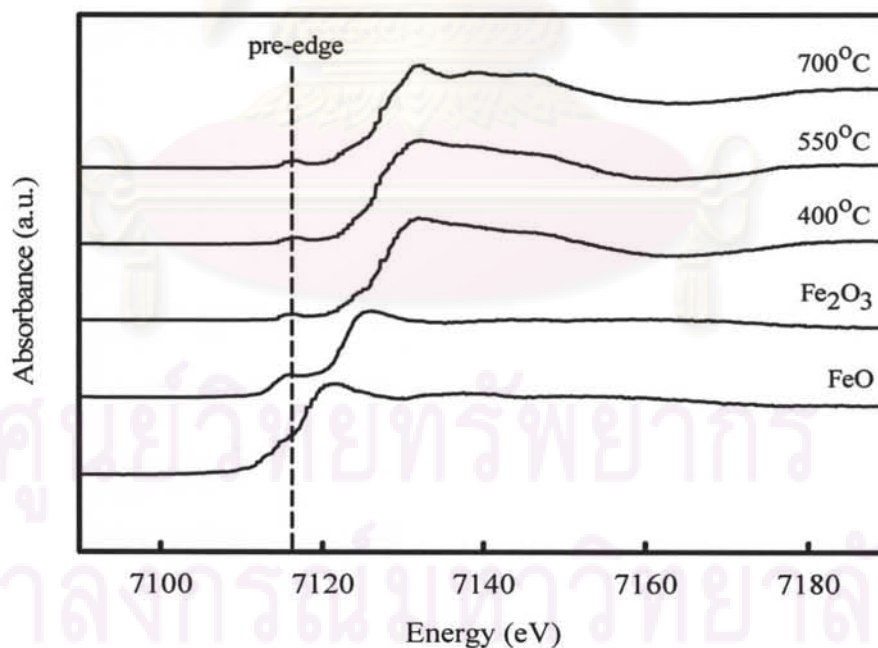


Figure 4.8 The XANES spectra of doped samples at different Fe contents, calcined at 400°C, and references FeO and Fe_2O_3 .

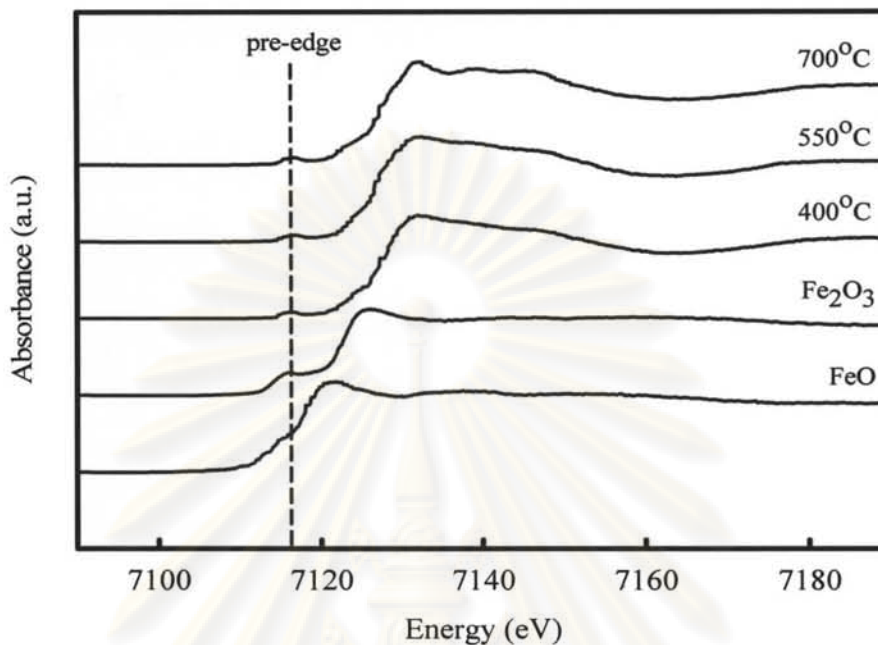


Figure 4.9 The XANES spectra of 5.0 mol% Fe-ZnO calcined at various temperature, and references FeO and Fe₂O₃.

4.1.6 Surface charge

Figure 4.10 and 4.11 show the zeta potential of all catalysts with respect to solution pH. The point where the plot passes through zero of zeta potential is called the zero point charge (pH_{zpc}). From Figure 4.10 and 4.11, it was found that the zeta potential changed from positive charge to negative charge at high pH. The pH_{zpc} of bare ZnO and Fe-ZnO samples are about 9.5 pH units shown in both Figures, which quite closes to the pH_{zpc} for ZnO (9.0) reported in the study of Akyol, Yatmaz, and Bayramoglu (2004). The pH_{zpc} of the samples did not shift according to both adding Fe and calcination temperature effect.

จุฬาลงกรณ์มหาวิทยาลัย

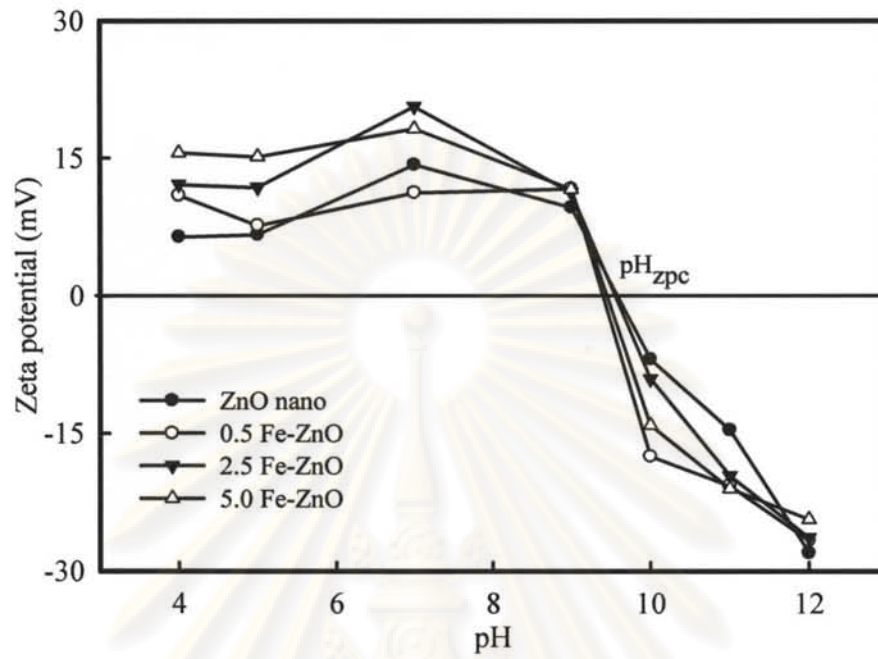


Figure 4.10 Plots of the zeta potential as a function of pH for bare ZnO and Fe-ZnO samples at difference Fe contents and calcined at 400°C.

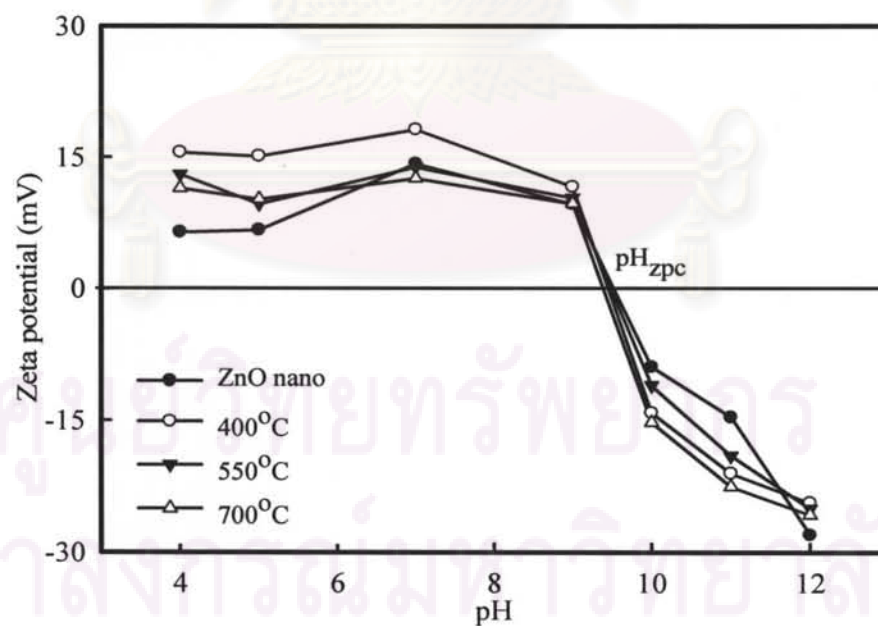
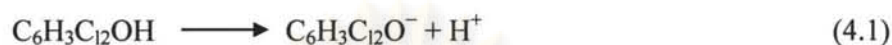


Figure 4.11 Plots of the zeta potential as a function of pH for bare ZnO and 5.0 mol% Fe-ZnO samples calcined at 400-700°C.

Catalyst surface presents positively when $\text{pH} < \text{pH}_{\text{zpc}}$, and negatively when $\text{pH} > \text{pH}_{\text{zpc}}$. The structure of pollutants also changes with the pH. As known, 2,4-DCP has its a pKa value of 7.89, presented by the following reaction.



When the pH of the solution is higher than its pKa, the pollutant exists mainly in anionic form. It can be inferred that more 2,4-DCP is adsorbed on catalysts surface at pH between the pKa of 2,4-DCP (7.89) and the pH_{zpc} (9.5) of the samples due to the opposite charge. Hence, our study began with fixed the pH of the reaction at 8.5.

4.2 Photocatalytic testing of 2,4-DCP

4.2.1 Experimental design analysis

In this work, three factor Box-Behnken design with a three central points under two replicate method was used to determine the operating conditions for maximizing the 2,4-DCP percent degradation. This statistical approach infers about three parameters effects (mol% Fe, calcination temperature, and catalyst loading) with a relatively small number of tests. Considering this design, 30 batches were recommended. In order to study following those recommended work, some parameters were fixed. These were 2,4-DCP concentration of 5 mg L^{-1} , pH 8.5, 1 h reaction time and 2 mM of $\text{K}_2\text{S}_2\text{O}_8$ was added for enhancing the degradation efficiency. The performing conditions and the responses were tabulated in Table 4.2. The percent degradation was considered as the response variables. The computed value at different factor level combinations was treated statistically to develop the response surface model.

Table 4.2 Box-Behnken design matrix and the response (% degradation).

Run order	Parameter			% degradation
	Fe (mol%)	Calcined temp. (°C)	Loading (g L ⁻¹)	
1	2.50	550	1.25	20.898
2	5.00	700	1.25	55.778
3	5.00	550	0.50	20.487
4	2.50	700	0.50	19.968
5	2.50	550	1.25	26.139
6	2.50	400	0.50	11.785
7	5.00	700	1.25	57.895
8	5.00	550	2.00	20.253
9	0.50	550	0.50	18.781
10	2.50	400	2.00	23.248
11	0.50	400	1.25	30.832
12	5.00	400	1.25	30.461
13	2.50	400	0.50	12.980
14	5.00	400	1.25	27.760
15	0.50	700	1.25	22.571
16	5.00	550	2.00	22.691
17	2.50	700	2.00	41.288
18	2.50	550	1.25	24.850
19	0.50	550	2.00	22.690
20	0.50	400	1.25	31.898
21	2.50	700	2.00	43.860
22	2.50	550	1.25	20.986
23	0.50	550	2.00	21.638
24	0.50	550	0.50	17.465
25	2.50	400	2.00	32.484
26	2.50	700	0.50	19.549
27	0.50	700	1.25	24.398
28	2.50	550	1.25	23.676
29	5.00	550	0.50	19.508
30	2.50	550	1.25	25.749

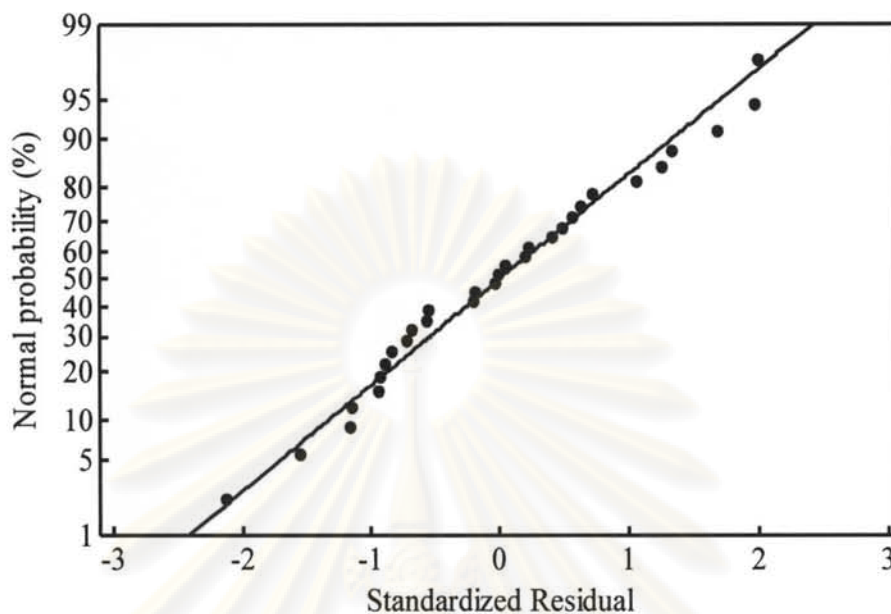


Figure 4.12 Normal probability plots.

4.2.1.1 Model validation

Generally, it is important to confirm the fitted model to make sure that it gives sufficient approximation to the actual test. Normal probability plot of the residual (Figure 4.12) was used to check the goodness of the model. The points in this plot should generally form a straight line if the residuals are normally distributed. If the points on the plot depart from a straight line, the normality assumption may be invalid. As the results shown in Figure 4.12, it was guaranteed that our experiment values would be in good agreement with predicted value.

Figure 4.13 presents a plot of standardized residuals against predicted response or fitted values. The plots of residuals versus fitted values showed a random scatter of residuals on both sides of zero, suggesting that the variance of original observations was assumed to be constant for all values of the response. This once proved that the established model was sufficient to estimate the degradation efficiency of 2,4-DCP.

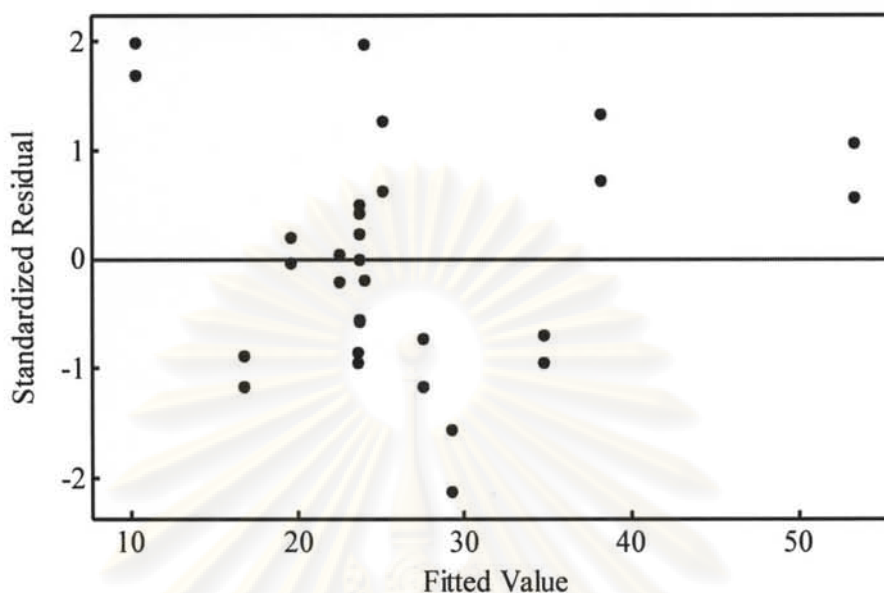


Figure 4.13 Plot of residual versus fitted value (predicted value).

Table 4.3 Estimated regression coefficients for % 2,4-DCP degradation.

Term	Coefficient	Standard error of coefficient	<i>p</i> -value
Constant	23.716	2.199	0.000
mol% Fe	4.035	1.346	0.007
calcined temp	5.241	1.346	0.001
loading	5.477	1.346	0.001
mol% Fe * mol% Fe	3.138	1.982	0.129
calcined temp * calcined temp	8.345	1.982	0.000
loading * loading	-6.416	1.982	0.004
mol% Fe * calcined temp	8.902	1.904	0.000
mol% Fe * loading	-0.642	1.904	0.740
calcined temp * loading	1.833	1.904	0.347

The computed regression coefficients for the model along with their respective *p*-value are presented in Table 4.3. Conventionally, at 95% confidence interval, the small *p*-values ($p < 0.05$) indicate the significance of the corresponding

coefficient. According to p -values we found that the terms are significant including mol% Fe, calcining temperature, and catalyst loading. While the interaction of mol% Fe and mol% Fe, mol% Fe and catalyst loading, and calcining temperature and catalyst loading are insignificant terms relating the p -values > 0.05 , which evidently observe in Table 4.3. The parameters considered in this study which shown in the table is expressed below.

$$\begin{aligned} \% \text{ degradation} = & 23.716 + (4.035 \times \text{mol\% Fe}) + (5.241 \times \text{calcined temp.}) \\ & + (5.477 \times \text{loading}) + 3.138 \times (\text{mol\% Fe})^2 + 8.345 \times \\ & (\text{calcined temp.})^2 - 6.416 \times (\text{loading})^2 + 8.902 \times (\text{mol\% Fe} \\ & \times \text{calcined temp.}) - 0.642 \times (\text{mol\% Fe} \times \text{loading}) + \\ & 1.833 \times (\text{calcined temp.} \times \text{loading}) \end{aligned} \quad (4.2)$$

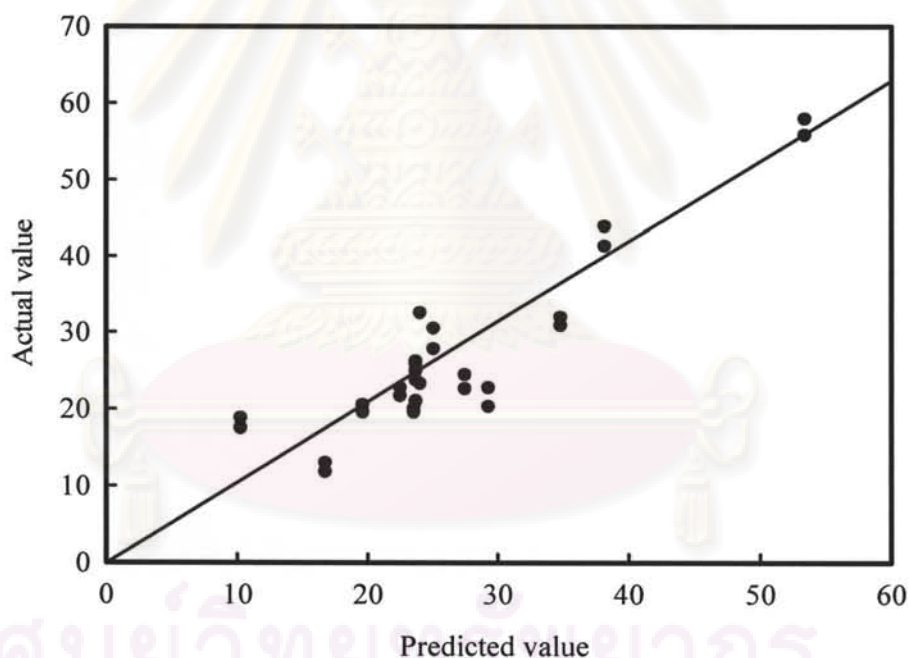


Figure 4.14 A parity plot of % degradation.

The actual and the predicted degradation plot are shown in Figure 4.14. It is observed that there are tendencies in the linear regression fit. It means that the regression model is adequately fitted with the actual values.

The quality of fitting the equation was expressed by the coefficient of determination (R^2). The R^2 values provide a measure of how much variability in the observed response values. It can be explained by the experimental factors and their interactions. The R^2 value is always between 0 and 1, if it closer to 1, the model is stronger and better to predicts the response. In this study, the value of R^2 is evaluated to 0.8281, implying that 82.81% of the variability in the response could be explained by the model. However, the adjusted determination coefficient (R^2_{adj}) is 0.7508, a little bit lower than the originated R^2 . This might be due to the result of the insignificance terms which shown in Table 4.3.

Table 4.4 ANOVA results for % degradation of 2,4-DCP.

Source	Degree of freedom	Sequential sum of square	F-value	p-value
Regression	9	2795.44	10.71	0.000
Linear	3	1179.95	13.56	0.000
Square	3	951.41	10.93	0.000
Interaction	3	664.08	7.63	0.001
Residual Error	20	580.11		
Pure Error	17	86.44		
Total	29	3375.56		

The results of analysis of variance (ANOVA) are shown in Table 4.4. ANOVA was used to check the significance and adequacy of the model. The Fischer's F test (F -value) is a statically valid measure of how well the factors describe the variation in the data about its mean (Liu and Chiou, 2005). It is the ratio of sum square regression to sum square residual error. The value greater than 4.0 is generally desirable. In this work, the ratio of sum square regression to sum square residual error turned to be 4.819 (2795.44/580.11). It was greater than 4.0 indicating that the model was adequate significantly for 2,4-DCP degradation.

The standardized residual for the batch run in our study is shown in Figure 4.15. The standardized residual was a measure of how much standard

derivation the actual value deviates from the predicted value. Most of the data should lie in the interval of ± 3.50 . Figure 4.15 illustrates that the value from our experiment was below the interval of ± 3.50 of standard residuals, which points to an approximation of the fitted model to the data has been good with no data recording error.

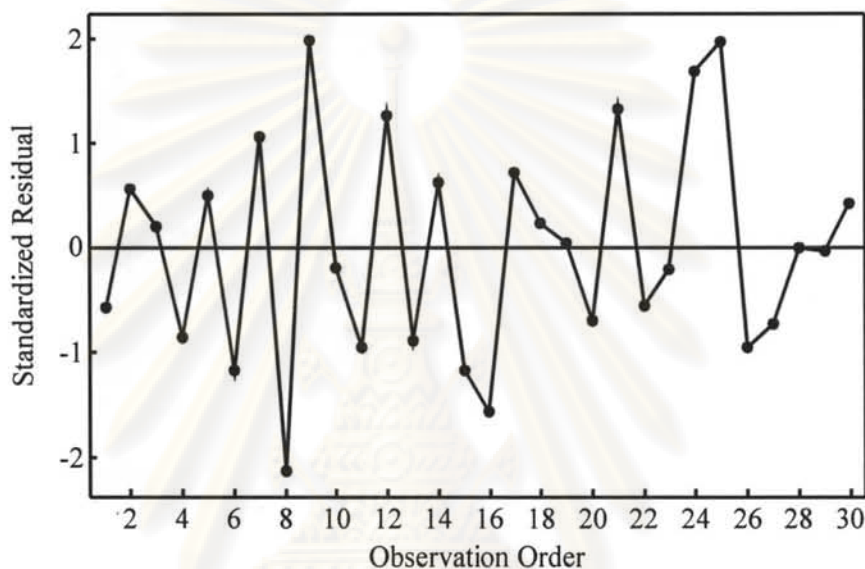


Figure 4.15 The standardized residual on each run.

4.2.1.2 Main effect investigation

The main effect plot on the response variable is shown in Figure 4.16. The results exhibited that increase mol% Fe doping tended to higher percent degradation. The plots exhibit that 5.0 mol% Fe present a highest degradation. The outcome correlated to the UV-DRS analysis i.e. 5.0 mol% Fe demonstrate the highest absorption in visible range.

Effect of calcination temperature was also examined and revealed that the degradation efficiencies of the catalyst calcined at 400 and 550°C were not significantly different. Obviously, the highest degradation efficiency could be observed for the catalyst calcined at 700°C. This result agreed to the XRD pattern

which showed that some metal or unstable phase could be taken out from ZnO at 700°C.

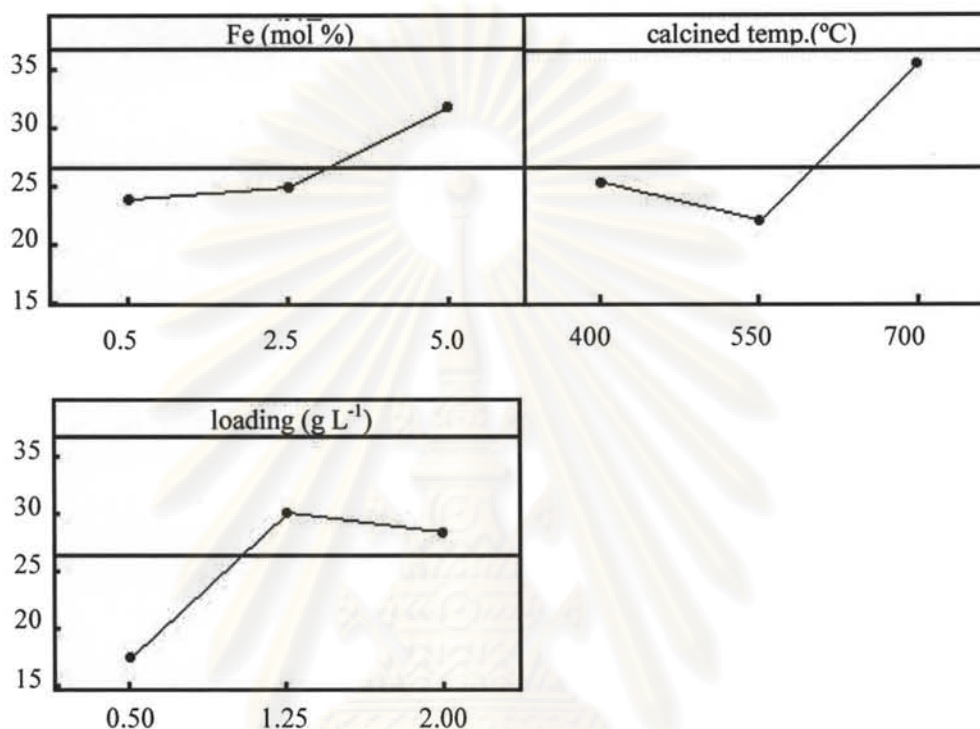
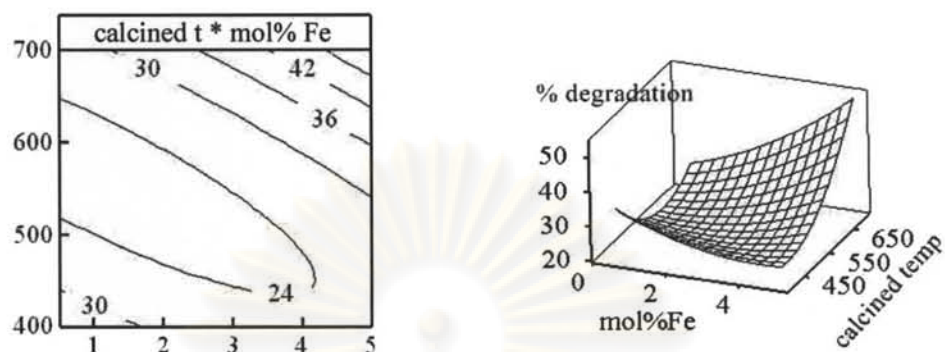


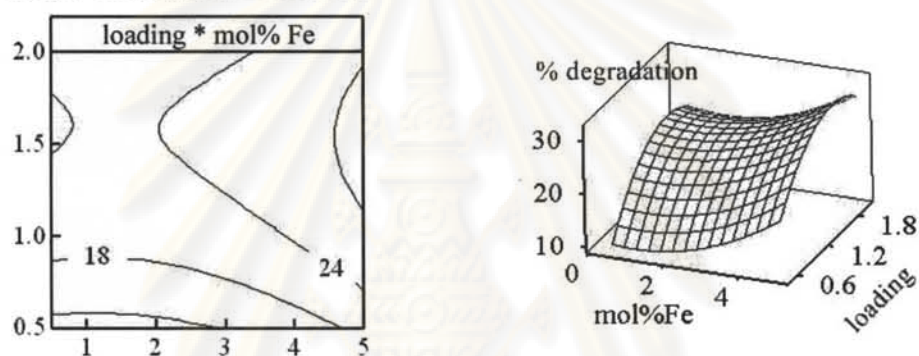
Figure 4.16 Main effect plots for % 2,4 DCP degradation.

The removal efficiency tended to be increased with increasing the catalyst loading from 0.5 to 1.25 g L⁻¹. However, the degradation efficiency slightly decreased when 2.0 g L⁻¹ of the catalyst loading was used. This is may be due to the fact that the increase in the number of catalyst particles will increase the number of photons absorbed and consequently the number of the 2,4-DCP molecule adsorbed. At high concentrations, photodegradation was somewhat decreased because of the aggregation of free catalyst particles resulting in a decrease in the number of surface active sites. Further, excess catalyst particles may lead to the excessive opacity and screening effect, consequently the light penetration was hindered.

(a) Calcination temperature and Fe content



(b) Catalyst loading and Fe content



(c) Catalyst loading and calcination temperature

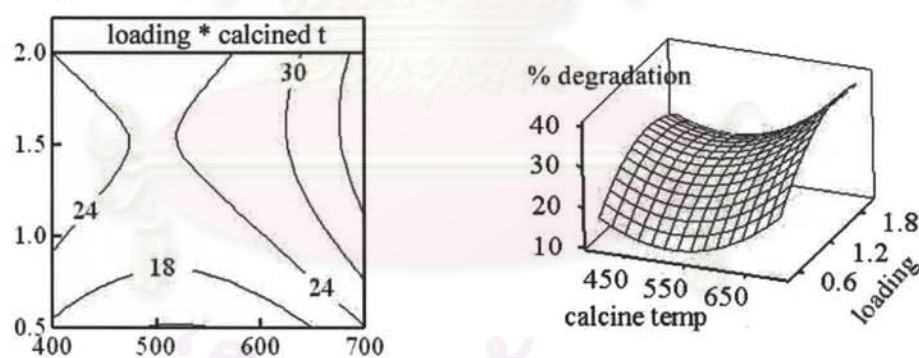


Figure 4.17 Contour plots and surface plots on different effects.

The study of the response surfaces and contour graphs provides a simple method to optimize the efficiency of the treatment and contributes to the identification of the interactions between the variables. The surface and contour plots

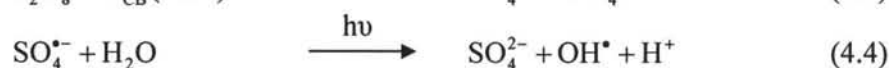
are given in Figure 4.17. The effect of calcination temperature and mol% Fe is shown in Figure 4.17(a). The high degradation efficiency was associated with high calcination temperature (680-700°C), and evaluated mol% Fe (4.5-5.0 mol%). Strong evidence of interaction between catalyst loading and mol% Fe is shown in Figure 4.17(b). Similarly, largest percent degradation was observed for high mol% Fe (4.5-5.0 mol%) as the catalyst loading in the level of 1.2-1.8 g L⁻¹. The data presented in Figure 4.17(c) describes the impact of catalyst loading and calcinations temperature. The plot revealed that the level of the catalyst loading in range of 1.2-2.0 g L⁻¹ was higher effective with calcining at high temperature (680-700°C).

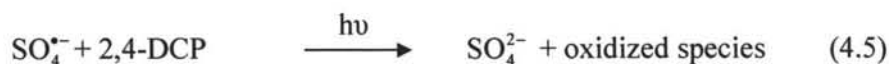
From the Box-Behnken analysis, the optimal operating parameter which was selected to apply further in the next our experiment was of 5.0 mol% Fe doped, calcined at 700°C, and the catalyst loading of 1.5 g L⁻¹.

4.2.2 Kinetic study

The optimal condition (5.0 mol% Fe-ZnO, calcined at 700°C, 1.5 g L⁻¹) obtained from the Box-Behnken analysis was selected to study the kinetics of 2,4-DCP photodegradation.

The study was carried out with 120 min. As the results shown in Figure 4.18, control experiment under illustrates that the degradation of 2,4-DCP was less than 4.0% under direct photolysis. Since photolysis effected the reaction insignificantly, the tests were then done in photoirradiation, as described in general. 2,4-DCP was hardly degraded in the present of 2 mM K₂S₂O₈ without catalysts i.e. less than 14.0% in 120 min. In the experiment using 5.0 mol% Fe-ZnO sample, the concentration of 2,4-DCP decreased about 7.0%, whereas the addition of 2 mM K₂S₂O₈ could enhance the degradation efficiency reached to 100% within 90 min. This probably could be explained via the following reactions:





The presence of $\text{S}_2\text{O}_8^{2-}$ was sufficient to oxidize 2,4-DCP in the presence of catalyst under visible light irradiation. This is because $\text{S}_2\text{O}_8^{2-}$ can generate the sulfate radical anions $\text{SO}_4^{\bullet-}$, which are very strong oxidizing species. Additionally, $\text{SO}_4^{\bullet-}$ increases the degradation efficiency by minimizing $e^- \cdot h^+$ recombination. In the experiment that used 5.0 mol% Fe-ZnO combined with $\text{K}_2\text{S}_2\text{O}_8$ (100%) exhibited higher degradation efficiency than 5 times of bare ZnO combined with $\text{K}_2\text{S}_2\text{O}_8$ (19.27%) at 90 min.

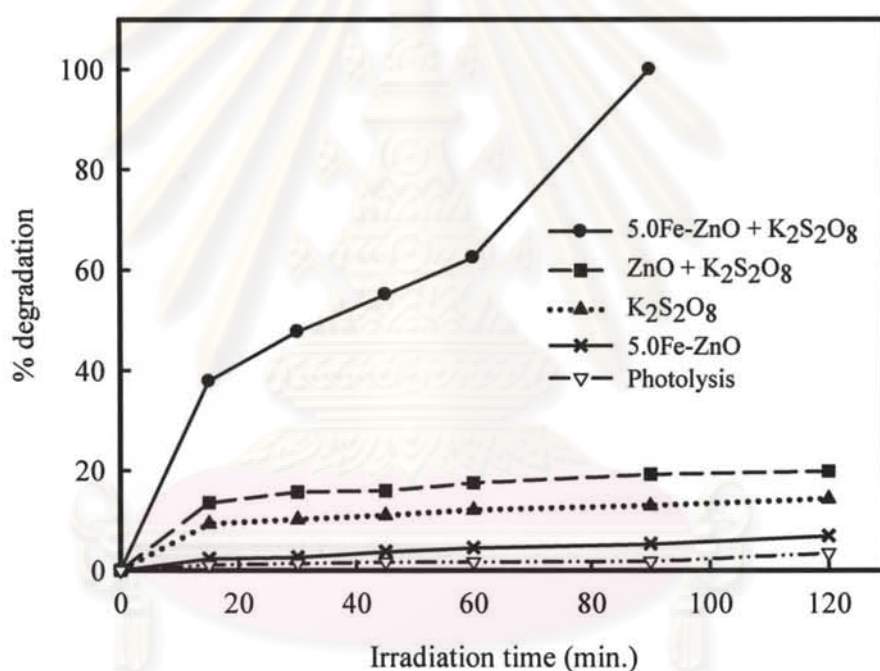
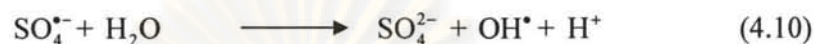
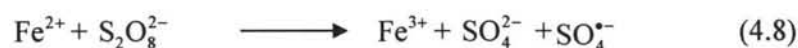
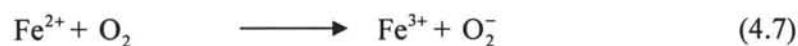
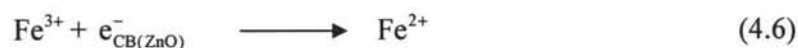


Figure 4.18 % degradation of 2,4-DCP under various conditions.
(Control parameters: 5.0 mg L⁻¹ of 2,4-DCP, 1.5 g L⁻¹ of catalyst, pH 8.5, 120 min.)

The experimental results show that doping with Fe^{3+} improved the photo-efficiency. It could be assumed that positively charged metal ions adsorbed on ZnO surface. It was easily reduced by e^- in conduction band, and thus increases the charge separation as given by following reaction (Naeem and Ouyang, 2009):



The enhancement of degradation by addition of Fe^{3+} ion was due to the electron scavenger effect of Fe^{3+} , which prevented the e^-h^+ recombination results in increase of the efficiency of photodegradation process.

From the results, we ensure that 5.0 mol% Fe-ZnO is an optimal catalyst. In this section, initial concentration of 2,4-DCP is investigated. The experiments were performed at different initial 2,4-DCP concentrations (5.0, 7.5, 10.0, 12.5, and 15.0 mg L^{-1}), while other parameters were maintained constant. The constant factors consisted of 1.5 g L^{-1} of 5.0 mol% Fe-ZnO, calcined 700°C, 2 mM $\text{K}_2\text{S}_2\text{O}_8$, pH 8.5, and 120 min reaction time.

The results in Figure 4.19 show that the maximum degradation (100%) is obtained within 90 min for low 2,4-DCP concentration (5.0 mg L^{-1}). At 90 min of reaction, the degradation efficiency decreased to 77.58, 63.26, 60.30, and 46.33% when increase the concentration in the level of 7.5, 10.0, 12.5, and 15.0 mg L^{-1} respectively.

We could deduce that, at low 2,4-DCP levels, the degradation efficiency was higher than that of higher concentration. This is probably due to the decrease in the ratio of OH^{\bullet} to 2,4-DCP molecules as a consequence of the increase in the 2,4-DCP concentration.

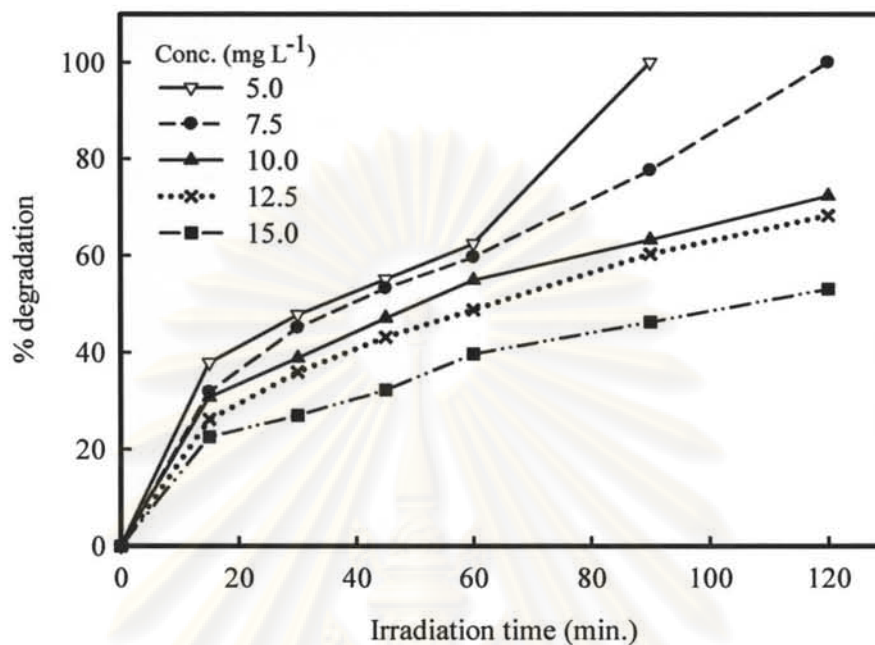


Figure 4.19 % degradation of 2,4-DCP of 5.0 mol% Fe-ZnO at different initial concentrations. (Conditions: 1.5 g L⁻¹ of catalyst, 2 mM K₂S₂O₈, pH 8.5, 120 min.)

This study applied the three point numerical differentiation formulas (Equation 4.11) to find the initial degradation rate (r_0) for each initial concentration (Fogler, 2006).

$$r_0 = \frac{-3C_{A0} + 4C_{A1} - C_{A2}}{2\Delta t} \quad (4.11)$$

Where: r_0 = initial degradation rate (min⁻¹)
 C_A = concentration of 2,4-DCP at reaction time t (mg L⁻¹)
 Δt = $t_{A2} - t_{A1}$ (min.)

Langmuir-Hinshelwood rate equation (Equation 4.12) have been used to determine the relationship between the initial degradation rate ($1/r_0$) and the initial equilibrium concentration of 2,4-DCP ($1/C_0$).

$$\frac{1}{r_0} = \frac{1}{k_r K_{ad} C_0} + \frac{1}{k_r} \quad (4.12)$$

where: k_r = reaction rate constant ($\text{mg L}^{-1} \text{min}^{-1}$), obtained by a linear plot of $1/r_0$ vs $1/C_0$

K_{ad} = the adsorption equilibrium constant (L mg^{-1})

C_0 = initial equilibrium concentration of 2,4-DCP (mg L^{-1})
(adsorption equilibrium concentration in the dark in this paper)

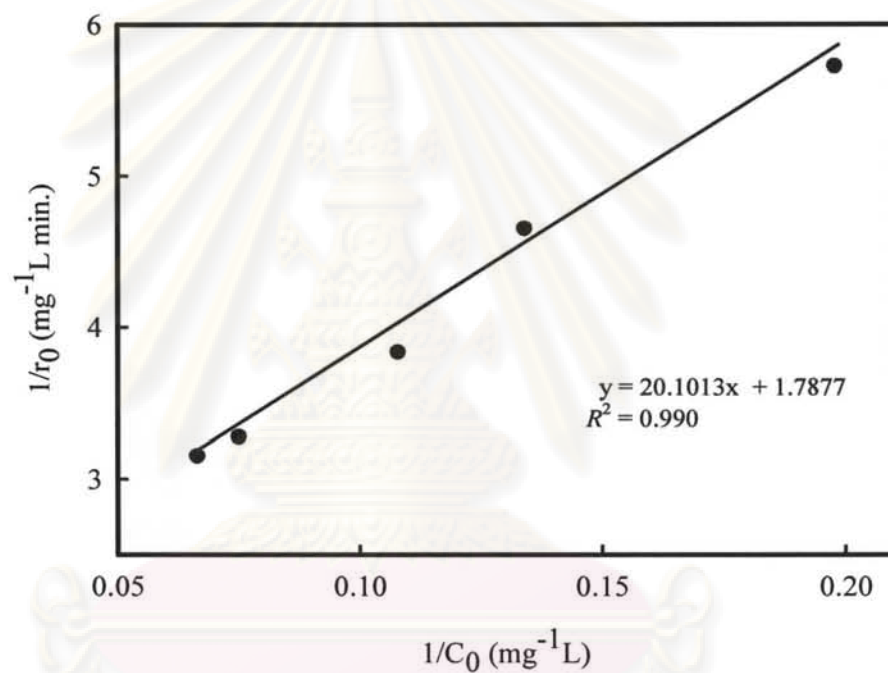


Figure 4.20 Langmuir-Hinshelwood plot depicting linear relationship between $1/r_0$ and $1/C_0$.

From the Langmuir-Hinshelwood plot shown in Figure 4.20, the linearity of this plot can be used to determine the adsorption constant (K_{ad}), and reaction rate constant (k_r). They are equal to 0.089 L mg^{-1} , and $0.559 \text{ mg L}^{-1} \text{ min}^{-1}$, respectively.

The results above demonstrate that the kinetics of 2,4-DCP photocatalytic degradation under our experimental conditions follows well the Langmuir-Hinshelwood rate equation ($R^2 = 0.990$).



ศูนย์วิทยทรัพยากร
จุฬาลงกรณ์มหาวิทยาลัย

CHAPTER V

CONCLUSIONS AND RECOMMENDATIONS

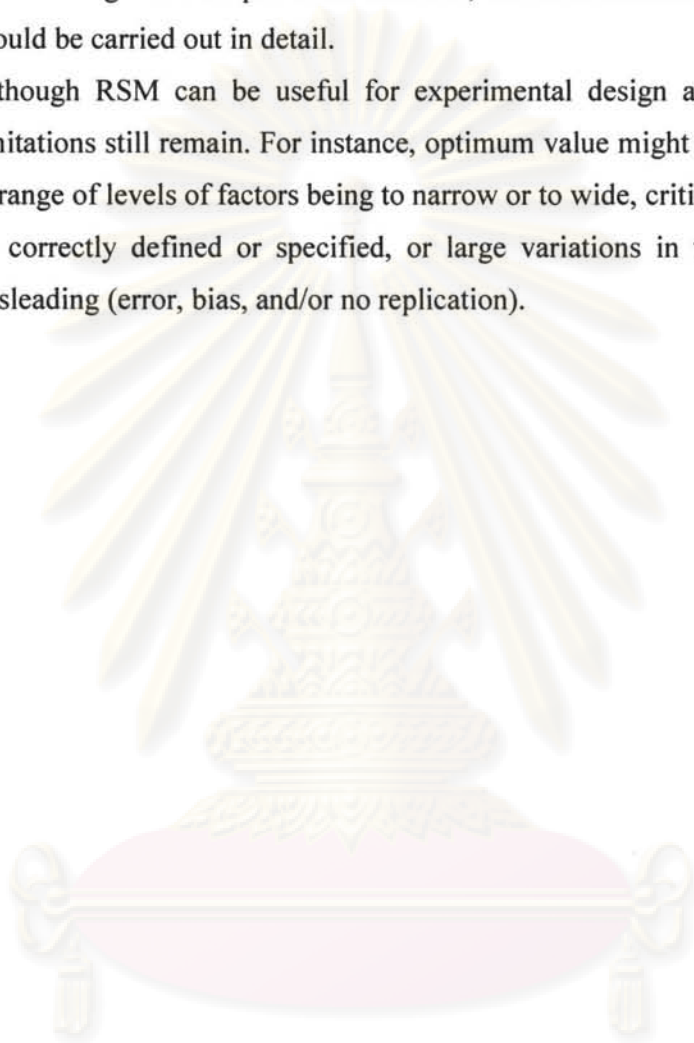
5.1 Conclusions

Fe-ZnO catalysts were successfully prepared by impregnation method. They were characterized by XRD, BET surface area, UV-DRS, XANES, and zeta potential. The study of 2,4-DCP photocatalytic reaction in visible light source was carried out based on Box-Behnken design of experiment, and further on kinetics in the Langmuir-Hinshelwood model. The conclusions could be drawn out as follows;

- 1) Fe-ZnO was prepared by impregnation technique providing the specific surface area (S_{BET}) range of $\sim 5-10 \text{ m}^2 \text{ g}^{-1}$. Fe species in Fe^{3+} form existed on the surface of ZnO. Its surface morphology was presented in rectangular chunk shape with average crystalline size of $\sim 35-40 \text{ nm}$.
- 2) The doping of Fe increased visible light absorption. This was probably due to Fe act as e^- transfer from valence band of ZnO to valence band of Fe_2O_3 .
- 3) The study of 2,4-DCP photodegradation based on Box-Behnken design of experiment provided an optimal conditions. Under fixed parameters of 25°C , pH 8.5, and $2 \text{ mM K}_2\text{S}_2\text{O}_8$ as an oxidant, the best condition was observed at Fe loading of $4.5-5.0 \text{ mol}\%$, calcined at $680-700^\circ\text{C}$, and with catalyst loading of $1.2-1.8 \text{ g L}^{-1}$. The statistical ANOVA data showed a high coefficient of determination value ($R^2 = 0.828$).
- 4) The 2,4-DCP photodegradation kinetics study was carried out under the best condition obtained from DOE. Its degradation rate was found to followed the Langmuir-Hinshelwood model ($R^2 = 0.990$). The activity of 5.0Fe-ZnO combined with $\text{K}_2\text{S}_2\text{O}_8$ was greater than that of commercial ZnO combined with $\text{K}_2\text{S}_2\text{O}_8$ about 5 times.
- 5) Addition of $2 \text{ mM K}_2\text{S}_2\text{O}_8$ increased the photocatalytic efficiency of 2,4-DCP (5.0 mg L^{-1}) significantly.

5.2 Recommendations

- 1) Since the effectiveness of photocatalysis was based on the adsorption capacity on the surface, catalyst modified for higher surface area should be attractive.
- 2) The investigations on pH of the solution, and electron acceptor concentration should be carried out in detail.
- 3) Although RSM can be useful for experimental design and analysis, some limitations still remain. For instance, optimum value might not be defined due to range of levels of factors being too narrow or too wide, critical factors may not be correctly defined or specified, or large variations in the factors can be misleading (error, bias, and/or no replication).



ศูนย์วิจัยทรัพยากร
จุฬาลงกรณ์มหาวิทยาลัย

REFERENCES

- Agency for Toxic Substances and Disease Registry (ATSDR). Toxicological profile for chlorophenols. [Online]. 1999. Available from : <http://www.atsdr.cdc.gov/toxprofiles/tp107.html> [2009, November 2]
- Akyol, A., Yatmaz, H.C., and Bayramoglu, M. Photocatalytic decolorization of remazol red RR in aqueous ZnO suspensions. Environmental 54 (2004): 19-24.
- Baek, S., Song, J., and Lim, S. Improvement of the optical properties of ZnO nanorods by Fe doping. Journal of Physical B 399 (2007): 101-104.
- Bayarri, B., Giménez, J., Curcó, D., and Esplugas, S. Photocatalytic degradation of 2,4-dichlorophenol by TiO₂/UV: Kinetics, actinometries and models. Catalysis Today 101 (2005): 227-236.
- Bera, A., and Basak, D. Photoluminescence and photoconductivity of ZnS-coated ZnO nanowires. Applied Materials & Interfaces 2 (2010): 408-412.
- Bezerra, M.A., Santelli, R.E., Oliveira, E.P., Villar, L.S., and Escalera, L.A. Response surface methodology (RSM) as a tool for optimization in analytical chemistry. Talanta 76 (2008): 965-977.
- Boonyatumanond, R., Jaksakul, A., Boonchalermit, S., Pancharoen, P., and Tabucanon, M.S. Monitoring of endocrine disruptor compounds in the coastal hydrosphere of Thailand. [Online]. 2003. Available from : <http://landbase.hq.unu.edu/Monitoring/Countryreports/Thailand/final%20data%20report%20UNU.htm> [2010, May 1]
- Centers for Disease control and Prevention (CDC). Occupational fatalities associated with 2,4-dichlorophenol (2,4-DCP) exposure, 1980-1998. [Online]. 2000. Available from : <http://www.cdc.gov/mmwr/preview/mmwrhtml/mm4923a3.htm> [2009, November 2]

- Chang, H., and Tsai, M.H. Synthesis and characterization of ZnO nanoparticles having prism shape by a novel gas condensation process. Reviews on Advanced Materials Science 18 (2008): 734-743.
- Chatterjee, D., and Dasgupta, S. Visible light induced photocatalytic degradation of organic pollutants. Photochemistry reviews 6 (2005): 186-205.
- Chen, C., Teo, K.L., Chong, T.C., Wu, Y.H., Osipowicz, T., and Rahman, M.A. Epitaxial growth of co-doped Eu and Sm in α -Zn_{0.05}Sr_{0.95}S on (001)MgO substrate using α -MnS buffer layer. Journal of Crystal Growth 264 (2004): 58-63.
- Cheng, P., Li, W., Zhou, T., Jin, Y., and Gu, M. Physical and photocatalytic properties of zinc ferrite doped titania under visible light irradiation. Chemistry 168 (2004): 97-101.
- Daneshvar, N., Salari, D., and Khataee, A.R. Photocatalytic degradation of azo dye acid red 14 in water on ZnO as an alternative catalyst to TiO₂. Chemistry 162 (2004): 317-322.
- De Lasa, H., Serrano, B., and Salaiques, M. Photocatalytic reaction engineering. United States of America: Springer Science+Business media, 2005.
- Dindar, B., and Icli, J. Unusual photoreactivity of zinc oxide irradiated by concentrated sunlight. Chemistry 140 (2001): 263-268.
- Dow AgroSciences. Material Safety Data Sheet (MSDS). [Online]. 2006. Available from : <http://www.cdms.net/ldat/mp6M3003.pdf> [2009, November 3]
- Fogler, H.S. Elements of chemical reaction engineering, Fourth edition. United States of America: Person education, 2006.
- Gao, J., Liu, L., Liu, X., Zhou, H., Huang, S., and Wang, Z. Levels and spatial distribution of chlorophenols-2,4-Dichlorophenol, 2,4,6-trichlorophenol, and pentachlorophenol in surface water of China. Chemosphere 71 (2008): 1181-1187.

- Gouvêa, C.A.K., Wypych, F., Moraes, S.G., Duran, N., Nagata, N., and Peralta-Zamora, P. Semiconductor-assisted photocatalytic degradation of reactive dyes in aqueous solution. Chemosphere 40 (2000): 433-440.
- Ha, S.R., and Vinitnantharat, S. Competitive removal of phenol and 2,4-dichlorophenol in biological activated carbon system. Environmental Technology 21 (2000): 387-396.
- International Agency for Research on Cancer (IARC). Volume 71 Re-evaluation of some organic chemicals, hydrazine and hydrogen peroxide. [online]. 1999. Available from : <http://monographs.iarc.fr/ENG/Monographs/vol71/volume71.pdf> [2009, November 4]
- Jung, M.W., et al. Adsorption characteristics of phenol and chlorophenols on granular activated carbons (GAC). Microchemical Journal 70 (2001): 123-131.
- Kabra, K., Chaudhary, R., and Sawhney, R.L. Treatment of hazardous organic and inorganic compounds through aqueous phase photocatalysis: a review. Industrial & Engineering Chemistry Research 43 (2004): 7683-7696.
- Kansal, S.K., Singh, M., and Sud, D. Optimization of process parameters for the photocatalytic degradation of 2,4-dichlorophenol in aqueous solutions. International Journal of Chemical Reactor Engineering 7 (2009): 1-24.
- Khodja, A.A., Sehili, T., Pihichowski, J.F., and Boule, P. Photocatalytic degradation of 2-phenylphenol on TiO₂ and ZnO in aqueous suspensions. Chemistry 141 (2001): 231-239.
- Kim, K.J., and Ahn, H.G. Complete oxidation of toluene over bimetallic Pt-Au catalysts supported on ZnO/Al₂O₃. Environmental 91 (2009): 308-318.
- Lathasree, S., Rao, A.N., SivaSankar, B., Sadasivam, V., and Rengaraj, K. Heterogeneous photocatalytic mineralisation of phenols in aqueous solutions. Chemical 223 (2004): 101-105.

- Li, D., and Haneda, H. Morphologies of zinc oxide particles and their effects on photocatalysis. Chemosphere 51 (2003): 129-137.
- Litter, M.I. Review Heterogeneous photocatalysis transition metal ions in photocatalytic systems. Environmental 23 (1999): 89-114.
- Liu, H.L., and Chiou, Y.R. Optimal decolorization efficiency of Reactive Red 239 by UV/TiO₂ photocatalytic process coupled with response surface methodology. Chemical Engineering Journal 112 (2005): 173-179.
- Lü, X., Lü, N., Gao, J., Jin, X., and Lü, C. Synthesis and properties of ZnS/polyimide nanocomposite films. Polymer international 56 (2007): 601-605.
- Maensiri, S., Laokul, P., and Promarak, V. Synthesis and optical properties of nanocrystalline ZnO powders by a simple method using zinc acetate dihydrate and poly (vinyl pyrrolidone). Journal of Crystal Growth 289 (2006): 102-106.
- Martani, E., and Seto, M. Degradation of 2,4-dichlorophenol in the microbial community of groundwater sample by bacteria isolate E-6. Journal of Pesticide Science 16 (1991): 429-434.
- Murphy, A.B. Band-gap determination from diffuse reflectance measurements of semiconductor films, and application to photoelectrochemical water-splitting. Solar Energy Materials & Solar Cells 91 (2007): 1326-1337.
- Naeem, K., and Ouyang, F. Parameter effect on heterogeneous photocatalysed degradation of phenol in aqueous dispersion of TiO₂. Journal of Environmental Sciences 21 (2009): 527-533.
- Naeem, K., and Ouyang, F. Preparation of Fe³⁺-doped TiO₂ nanoparticles and its photocatalytic activity under UV light. Physica B 405 (2010): 221-226.
- Nahar, M.S., Hasegawa, K., and Kagaya, S. Photocatalytic degradation of phenol by visible light-responsive iron-doped TiO₂ and spontaneous sedimentation of the TiO₂ particles. Chemosphere 65 (2006): 1976-1982.

- Navío, J.A., et al. Heterogeneous photocatalytic reactions of nitrite oxidation and Cr(VI) reduction on iron-doped titania prepared by the wet impregnation method. Environmental 16 (1998): 187-196.
- Özgür, Ü., et al. A comprehensive review of ZnO materials and devices. Journal of Applied Physics 98 (2005): 1-103.
- Pardeshi, S.K., and Patil, A.B. A simple route for photocatalytic degradation of phenol in aqueous zinc oxide suspension using solar energy. Solar Energy 82 (2008): 700-705.
- Park, S.B., and Kang, Y.C. Photocatalytic activity of nanometer size ZnO particles prepared by spray pyrolysis. Journal of Aerosol Science 28 (1997): 473-474.
- Pesticide Action Network (PAN) Germany. PAN international list of highly hazardous pesticides. [Online]. 2009. Available from : http://www.pan-germany.org/download/PAN_HHP-List_090116.pdf [2009, November 3]
- Pollution Control Department (PCD). Water quality standards. [Online]. 2004. Available from : http://www.pcd.go.th/info_serv/en_reg_std_water.html [2010, May 1]
- Porambo, M.W., Howard, H.R., and Marsh, A.L. Dopant effects on the photocatalytic activity of colloidal zinc sulfide semiconductor nanocrystals for the oxidation of 2-chlorophenol. Journal of Physical Chemistry C 114 (2010): 1580-1585 .
- Poulios, I., Makri, D., and Prohaska, X. Photocatalytic treatment of olive milling waste water, oxidation of protocatechuic acid. Global Nest: The International Journal 1 (1999): 55-62.
- Quan, X., Shi, H., Liu, H., Lv, P., and Qian, Y. Enhancement of 2,4-dichlorophenol degradation in conventional activated sludge systems bioaugmented with mixed special culture. Water Research 38 (2004): 245-253.

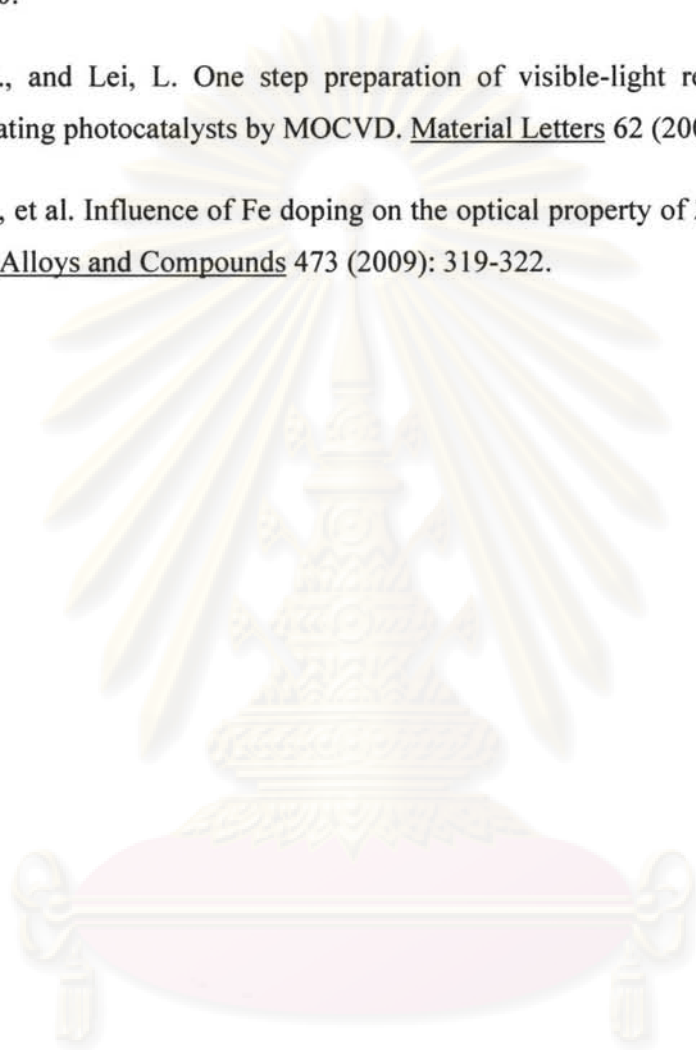
- Rao, N.N., Dubey, A.K., Mohanty, S., Khare, P., Jain, R., and Kaul, S.N. Photocatalytic degradation of 2-chlorophenol: a study of kinetics, intermediates and biodegradability. Journal of Hazardous Materials B 101 (2003): 301-314.
- Roggenbuck, J., Waitz, T., and Tiemann, M. Synthesis of mesoporous metal oxides by structure replication: Strategies of impregnating porous matrices with metal salts. Microporous and Mesoporous Materials 113 (2008): 575-582.
- Sakthivel, S., Neppolian, B., Shankar, M.V., Arabindoo, B., Palanichamy, M., and Murugesan, V. Solar photocatalytic degradation of azo dye : comparison of photocatalytic efficiency of ZnO and TiO₂. Solar Energy Materials & Solar Cells 77 (2003): 65-82.
- Salah, N.H., Bouhelassa, M., Bekkouche, S., and Boultif, A. Study of photocatalytic degradation of phenol. Desalination 166 (2004): 347-354.
- Sharma, P.K., Dutta, R.K., Pandey, A.C., Layek, S., and Verma, S.L. Effect of iron doping concentration on magnetic properties of ZnO nanoparticles. Journal of Magnetism and Magnetic Materials 321 (2009): 2587-2591.
- Shifu, C., Wei, Z., Sujuan, Z., and Wei, L. Preparation, characterization and photocatalytic activity of N-containing ZnO powder. Chemical Engineering Journal 148 (2009): 263-269.
- Tayade, R.J., Kulkarni, R.G., and Jasra, R.V. Transition metal ion impregnated mesoporous TiO₂ for photocatalytic degradation of organic contaminants in water. Industrial & Engineering Chemistry Research 45 (2006): 5231-5238.
- Teoh, W.Y., Amal, R., Mädler, L., and Pratsinis, S.E. Flame sprayed visible light-active Fe-TiO₂ for photomineralisation of oxalic acid. Catalysis Today 120 (2007): 203-213.

- The European Commission. Annex 13: List of 146 substances with endocrine disruption classifications prepared in the Expert meeting. [Online]. 2001. Available from : http://ec.europa.eu/environment/docum/pdf/bkh_annex_13.pdf [2010, May 2]
- UK Marine Special Areas of Conservation (UK Marine SACs). Chlorophenols and dichlorophenols. [Online]. 2001. Available from : http://www.ukmarinesac.org.uk/activities/water-quality/wq8_36.htm [2009, November 3]
- United States Environmental Protection Agency (U.S.EPA). Ambient water quality criteria for 2,4-dichlorophenol. [Online]. 1980. Available from : <http://nepis.epa.gov/EPA/html/DLwait.htm?url=/Adobe/PDF/30006791.PDF> [2009, November 3]
- United States Environmental Protection Agency (U.S.EPA). National recommended water quality criteria: 2002. [Online]. 2002. Available from : <http://www.epa.gov/waterscience/criteria/wqctable/nrwqc-2002.pdf> [2009, November 3]
- Valli, K., and Gold, M.H. Degradation of 2,4-dichlorophenol by the lignin-degrading fungus *Phanerochaete chrysosporium*. Journal of Bacteriology 173 (1991): 345-352.
- Wang, R., Xin, J.H., Yang, Y., Liu, H., Xu, L., and Hu, J. The characteristics and photocatalytic activities of silver doped ZnO nanocrystallites. Applied Surface Science 227 (2004): 312-317.
- Wang, Y.S., Thomas, P.J., and O'Brien, P. Optical properties of ZnO nanocrystals doped with Cd, Mg, Mn, and Fe ions. The Journal of Physical Chemistry B 110 (2006): 21412-21415.
- Xiangzhong, L., Wei, Z., and Jincai, Z. Visible light-sensitized semiconductor photocatalytic degradation of 2,4-dichlorophenol. Science in China (series B) 45 (2002): 421-425.

Zhang, J.F, Liu, H., Sun, Y.Y., Wang, X.R., Wu, J.C., and Xu, Y.Q. Responses of the antioxidant defenses of the Goldfish *Carassius auratus* exposed to 2,4-dichlorophenol. Environmental Toxicology and Pharmacology 19 (2005): 185-190.

Zhang, X., and Lei, L. One step preparation of visible-light responsive Fe-TiO₂ coating photocatalysts by MOCVD. Material Letters 62 (2008): 895-897.

Zhang, Y., et al. Influence of Fe doping on the optical property of ZnO films. Journal of Alloys and Compounds 473 (2009): 319-322.



ศูนย์วิทยทรัพยากร
จุฬาลงกรณ์มหาวิทยาลัย



APPENDICES

ศูนย์วิทยทรัพยากร
จุฬาลงกรณ์มหาวิทยาลัย

APPENDIX A

The transmission spectrum of NaNO_2

A 500W xenon lamp emits both UV and visible light. To investigate photocatalytic activities of the prepared catalysts under visible light, the light beam was passed through 1M NaNO_2 solution to cut off wavelengths shorter than 400 nm. The transmission spectra of 1M NaNO_2 solution is presented in the figure below (Cheng et al., 2004).

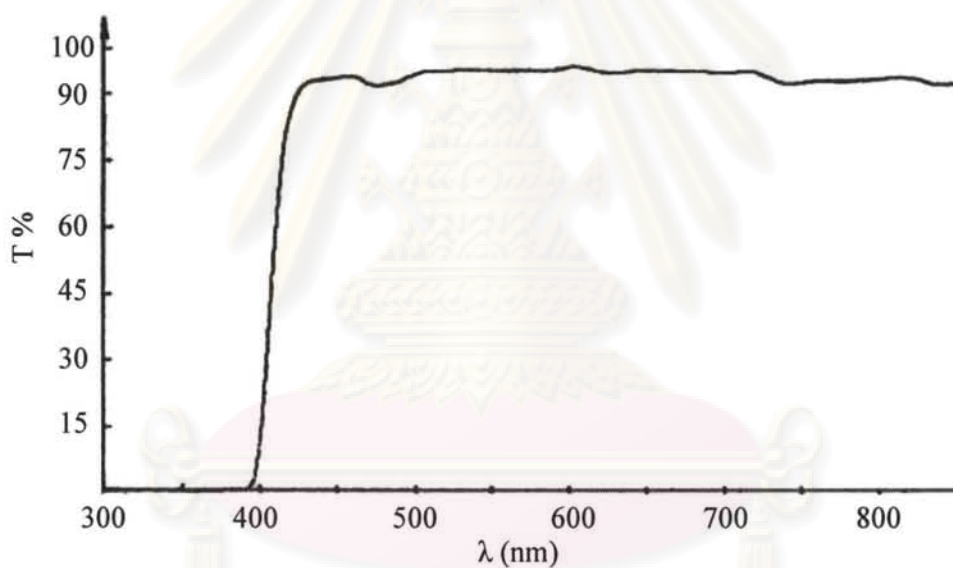


Figure A.1 The transmission spectrum of 1M NaNO_2 solution.

ศูนย์วิทยทรัพยากร
จุฬาลงกรณ์มหาวิทยาลัย

APPENDIX B

Characterization data

B.1 Crystal size calculation

Table B.1 Crystal sizes of the samples.

Sample	Calcined temp. (°C)	FWHM (degree)	β	$\cos\theta$	Crystal size (nm)
ZnO nano	-	0.2327	0.0041	0.9499	35.93
0.5Fe-ZnO	700	0.2225	0.0039	0.9497	37.58
2.5Fe-ZnO	700	0.2225	0.0039	0.9498	37.58
5.0Fe-ZnO	700	0.2215	0.0039	0.9499	37.74
5.0Fe-ZnO	550	0.2215	0.0039	0.9499	37.74
5.0Fe-ZnO	400	0.2326	0.0041	0.9497	35.95

B.2 XANES data

Table B.2 The pre-edge energy of the samples and model compounds (FeO, Fe₂O₃).

Sample	Calcined temp. (°C)	Pre-edge energy (eV)
FeO	-	7113.49
Fe ₂ O ₃	-	7115.81
0.5Fe-ZnO	400	7115.81
2.5Fe-ZnO	400	7115.81
5.0Fe-ZnO	400	7115.81
5.0Fe-ZnO	550	7115.81
5.0Fe-ZnO	700	7115.81

B.3 Zeta potential data

Table B.3 Average zeta potential (mV) of bare ZnO, and Fe-ZnO samples.

Sample	Calcined temp (°C)	Avg. Zeta potential (mV) at pH 4-12						
		4	5	7	9	10	11	12
ZnO nano	-	6.44	6.70	14.28	9.64	-6.90	-14.60	-28.00
0.5Fe-ZnO	400	10.96	7.68	11.24	11.65	-17.50	-20.70	-27.00
2.5Fe-ZnO	400	12.13	11.80	20.62	11.25	-9.05	-19.60	-26.30
5.0Fe-ZnO	400	15.58	15.14	18.20	11.61	-14.10	-21.00	-24.30
5.0Fe-ZnO	550	13.02	9.66	13.89	10.35	-11.00	-19.00	-25.00
5.0Fe-ZnO	700	11.45	10.19	12.58	9.71	-15.20	-22.50	-25.70

ศูนย์วิทยทรัพยากร
จุฬาลงกรณ์มหาวิทยาลัย

APPENDIX C

Photocatalytic testing data

C.1 Calibration curve of 2,4-DCP

Table C.1 Calibration curve data of 2,4-DCP

No.	Concentration (mg L ⁻¹)	Area
1	0.625	7.1
2	1.25	13.9
3	2.5	28.4
4	5.0	57.3
5	10.0	117.7
6	20.0	237.5
7	40.0	480.6

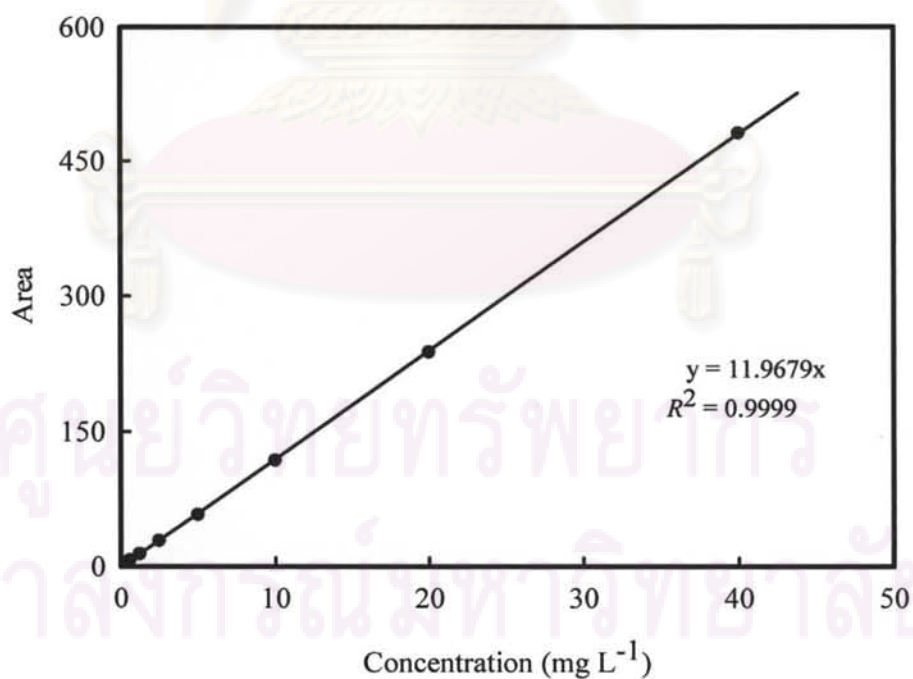


Figure C.1 Calibration curve of 2,4-DCP

C.2 % degradation

The photocatalytic efficiency of 2,4-DCP is calculated from the following formula:

$$\% \text{ degradation} = \left(\frac{C_0 - C_t}{C_0} \right) \times 100\% \quad (\text{C.1})$$

where: C_0 = the initial concentration of 2,4-DCP

C_t = the concentration of 2,4-DCP after irradiation time t .

Table C.2 % degradation of 5.0 mg L⁻¹ 2,4-DCP at various conditions.

Rx time (min.)	% degradation				
	2,4-DCP photolysis	5.0Fe-ZnO	K ₂ S ₂ O ₈	ZnO + K ₂ S ₂ O ₈	5.0Fe-ZnO + K ₂ S ₂ O ₈
0	0.00	0.00	0.00	0.00	0.00
15	1.08	2.36	9.30	13.54	37.89
30	1.38	2.67	10.20	15.73	47.79
45	1.68	3.77	10.99	15.98	55.16
60	1.68	4.55	12.10	17.56	62.44
90	1.77	5.33	12.95	19.27	100.00
120	3.44	6.91	14.33	19.88	

Table C.3 % degradation of 2,4-DCP at different concentrations.

Rx time (min.)	% degradation				
	5.0 mg L ⁻¹	7.5 mg L ⁻¹	10.0 mg L ⁻¹	12.5 mg L ⁻¹	15.0 mg L ⁻¹
0	0.00	0.00	0.00	0.00	0.00
15	37.89	31.92	30.85	26.18	22.59
30	47.79	45.15	38.88	35.98	27.04
45	55.16	53.29	47.14	43.18	32.29
60	62.44	59.73	54.96	48.82	39.74
90	100.00	77.58	63.26	60.30	46.33
120		100.00	72.32	68.24	53.09

BIOGRAPHY

Miss Pradabduang Kiattisaksiri was born on December 13, 1985 in Chaiyaphum province, Thailand. The author received her Bachelor Degree of Science in Health Science from Faculty of Science and Technology, Thammasat University in August, 2008. During a bachelor study, she was interested in participating in several extra-curricular activities. For example she was a participant in TU science camp 2005 and the 24th Universiade Bangkok sport game 2007. She had experiences in field training of safety and environment at Thai Bridgestone CO.,LTD, Rangsit factory, and Techno Resin CO.,LTD., Navanakorn factory. Her senior project was “The study of compressive strength of mortar congregated with aluminum dust”. Her interest is hazardous waste management and wastewater treatment.



ศูนย์วิทยทรัพยากร
จุฬาลงกรณ์มหาวิทยาลัย